INSTRUMENTS AND METHODS OF INVESTIGATION

Surface-plasma method for the production of negative ion beams

V G Dudnikov

Contents

Abstract. **Increased interest in the development of negative ions sources is related to the emergence of important applications of negative-ion beams. These are, first of all, tandem accelerators, high-energy implantation and accelerator-based mass spectrometry, supercollimated beams, charge-exchange injection into cyclic accelerators and storage rings, charge-exchange extraction of beams from cyclotrons, injectors of high-energy neutrals in plasma systems, and charge-exchange beam separation. The development of sources of negative ions and their use in academic research and industry are reviewed. Physical bases and designs of surface-plasma sources of negative ions, as well as the history of their development, are presented.**

Keywords: surface-plasma method, surface-plasma source, work function, negative ions, cesium, RF discharge

V G Dudnikov Novosibirsk State University,
ul. Pirogova 2, 630090 Novosibirsk, Russian Federation;
Budker Institute of Nuclear Physics, Siberian Branch of the Russian Academy of Sciences,
prosp. Akademika Lavrent'eva 11, 630090 Novosibirsk,
Russian Federation
E-mail: dvg43@yahoo.com

1. Introduction

The generation of positive ions in gas-discharge plasma, which was used in the first ion sources, also proved to be the most effective method for the production of positive ion beams [1]. Several modern modifications of this method provide a very high efficiency of producing positive-ion beams that is close to the theoretical limit. In most cases, the intensity of the obtained beams is limited by the capacities of ion-optical systems that form the beams rather than the capacities for generating ions. Because of this, efforts have been increasingly focused on formatting and accelerating ion beams. Positive ion sources have been developed with acceleration in plasma with a closed electron drift and compensating space charge [2].

The situation with methods for producing negative ion beams was quite different. The development of those methods significantly lagged behind both the progress in developing positive ion sources and the requirements of important and efficient applications. The most important applications of negative-ions beams employ efficient conversion of accelerated negative ions into fast atoms and positive ions. These applications exhibit some general features that are due to the use of the effects of the charge-exchange technique on flows of accelerated particles; owing to this, they can be combined into a charge-exchange technology for the production and use of beams of accelerated particles [3].

Before 1968, the intensity of negative ion beams obtained from sources of various kinds was limited, at a level of several

milliamperes, by constraints on generating negative ions. In 1971, the principal limitations on the attainable intensity of negative-ions beams were eliminated, as a result of which obtaining H$^-$ ion beams with a current of 1 A became feasible, while the generation of negative-ion beams with a significantly higher intensity became, to a large extent, a technical problem [4].

Progress in the production of negative-ion beams was related to developments in two areas: (1) a significant enhancement of the charge-exchange method for generating negative-ion beams using a positive-ion source with multi-aperture systems for beam formation along with the use of efficient targets made of alkali and alkaline earth metals and (2) the development of a basically new surface-plasma method (SPM) of negative-ion formation and development of efficient surface-plasma sources (SPSs) of negative ions. As a result of the intense search for new methods for the production of negative ion beams conducted at the Institute of Nuclear Physics of the Siberian Branch of the Russian Academy of Science at Novosibirsk (currently G I Budker Institute of Nuclear Physics of the Siberian Branch of the Russian Academy of Science), it was found in 1971 that adding cesium to a gas-discharge cell substantially increases the emission of negative ions from gas-discharge plasma [4]. Subsequent studies have shown that the higher yield of negative ions from the discharge is due to emission of negative ions from the surface of electrodes bombarded by gas discharge plasma particles enhanced in the presence of cesium [5]. Adsorption of cesium on the electrode surface lowers the surface work function from 4–5 eV to 1.6–2 eV. Negative ions are formed then due to the capture of electrons from the electrodes to electron-affinity levels of sputtered and back-scattered particles. In the same way, the emission of negative positronium and muonium ions [6, 7] is intensified by deposition of alkali metals on the surface of single-crystal tungsten. An efficient method was proposed in [8] to obtain ultracold negative muonium ions by electron capture by muonium atoms on the cesiated surface of single-crystal tungsten, palladium, and aerogel and due to the resonant charge exchange on positive and negative hydrogen ions.

The elementary processes of negative ion formation occurring if a solid surface is bombarded by fast particles were found experimentally by K S Woodcock as early as 1931 [9]. It was discovered by A Kh Ayukhanov in 1961 [10] and V Kron in 1962 [11] that the emission of secondary negative ions from the surface is increased in the case of adsorption of alkali metal films. However, the observed efficiency of the formation of negative ions with small electron affinity was low, and the intensities of negative-ion beams produced due to secondary emission were so small that these processes were not taken into account later in analyzing the formation of negative ions in ion sources nor were attempts made to employ them to generate intense beams of negative ions [1].

After charge-exchange injection was invented in 1967 [12], G I Budker proposed to develop a quality source of negative ions for accelerators. Three groups were organized at the Institute of Nuclear Physics to develop the sources: Roslyakov's group had to develop charge-exchange sources, Dimov's group secondary-emission sources, and Dudnikov's group plasma sources. In developing the plasma sources, cesiation effect was discovered, i.e., a significant increase in the emission of negative ions from the discharge and reduction in electron emission if vapors of cesium or other substances with a low ionization potential are added to the discharge [4]. The cesiation effect has become a basis for developing a new method of surface plasma production of negative-ion beams [5, 13].

2. Discovery of the cesiation effect

After numerous experiments with a variety of designs of negative-ion sources with discharges in cylindrical and planar magnetrons filled with various hydrogen-containing gases performed in early 1971, studies of the emission of negative ions from hydrogen plasma discharges in crossed electric and magnetic fields were resumed. Given the acquired 'negative' experience gained in a number of trial experiments, the design of the new source was brought to the form depicted schematically in Fig. 1.

A plasma cell casing (3) was fixed on plexiglass insulators (2) in the gap between pole tips (1). The plates of an extraction

Figure 1. Schematic of negative ion beam production from a gas-discharge cell with the planotron configuration [13]: *1* — electromagnet pole tips, *2* — high-voltage insulators, *3* — gas-discharge chamber casing, *4* — pulsed gas inlet valve, *5* — anode insert, *6* — emission slit screens, *7* — emission slit, *8* — collector, *9* — negative ion beam, *10* — central cathode plate, *11* — cathode side shields, *12* — cathode holders, *13* — cathode insulators, *14* — extractor plates.

electrode (*14*) were welded to special protrusions of pole tips (*1*) that create in the high-voltage gap a magnetic field with a trap-free configuration.

A pair of pole tips with the source was installed between the grounded poles of an electromagnet. A gas-discharge cell with a planotron configuration consists of a cathode that contains a central plate (*10*), side plates (*11*), and a cathode-enclosing anode that consists of parts of the gas-discharge cell casing (*3*) and anode insert (*5*). The cathode, made of 0.2-mm-thick tantalum tape, was attached to current leads (*12*) made of tantalum wire that passed through the wall of the anode insert (*5*) and were insulated from it by ceramic tubes (*13*). The volume of the gas-discharge cell was reduced to the minimum. The gaps between the cathode and the anode, in which the discharge should not burn, were reduced to 1 mm. Hydrogen was supplied to the gas-discharge cell through a short channel by a pulsed electromagnetic valve (*4*). An emission slit (*7*) with dimensions of 0.5×10 mm oriented across the magnetic field was cut in the thin wall of the gas-discharge cell casing. Particles could pass from the discharge region to the emission slit through the gap between the anode emission slit screens (*6*) that shield the emission slit from the dense high-current discharge plasma. Hydrogen was supplied, discharge ignited, and ions extracted using the power supply systems employed earlier. A beam collector (*8*) was installed to detect a beam (*9*) below the source. The negative-polarity extraction voltage was now applied to the gas-discharge cell casing, while the collector was maintained under a low voltage.

A photo of the first planotron is shown in Fig. 2. After some initial testing, the source operation mode was found in which a pulsed discharge with rectangular 1-ms-long current pulses exhibited sustainable burning at a discharge current of up to $I_p \sim 30$ A. The discharge voltage drop was kept about $U_p \sim 400$ V when the discharge current, hydrogen supply, and magnetic field strength were widely varied. Under optimum conditions, a negative ion beam with a collector current of up to $I^- \sim 4.5$ mA was obtained from these sources with an extraction voltage of $U_0 \sim 20$ kV. The total current in the extraction circuit was in this case no greater than $I_0 \sim 15$ mA. This implies that the parasitic current due to accompanying electrons and all other processes only exceeded the negative ion beam current by a factor of two, whereas in all earlier negative-ion sources the electron current exceeded the ion beam current by a factor of tens or hundreds.
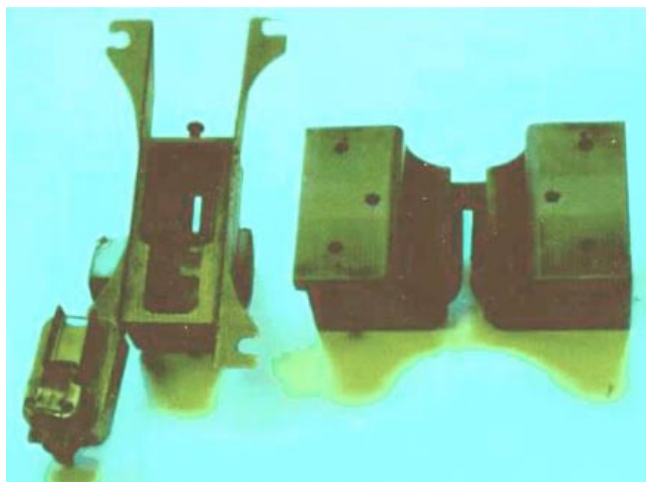
Thus, hopes to decrease the flow of accompanying electrons by decreasing the length of the emission gap along the magnetic field were reinforced.

The sustainable operation of the source rekindled interest in nonstandard methods of enhancing the generation of negative ions. First of all, we wanted to test how cesium vapor affected the formation of H^- ions in the source discharge. The first experiments of this kind were performed on July 1, 1971. A tablet made of a pressed mixture of cesium chromate and titanium that contained 1 mg of releasable cesium was attached to the side wall of the anode insert facing the discharge. It was assumed that cesium would be released into the discharge when the tablet was heated by the plasma. In this experiment, the dimensions of the gap between the anode emission slit screens, through which the plasma particles passed to the emission slit, were 0.7×10 mm. A beam of H^- ions with current $I^- = 1.5$ mA arrived at the collector for approximately the same discharge parameters. After awhile, the collector current at the end of the pulse began increasing as shown in Fig. 3. The current pulse acquired an almost triangular shape: the collector current increased during the pulse from $I^- = 1.5$ mA to $I^- = 4$ mA. After 20 minutes of source operation at a repetition rate of 3 Hz, the surge on the trailing edge disappeared, and the oscillogram acquired an ordinary rectangular shape with the amplitude $I^- = 1$ mA. An assumption was made that the surge in the collector current was associated with the release of cesium into the discharge.

Cathodes are heated in the plasma discharges under investigation much more than the anodes. Therefore, the cesium tablets were fixed in subsequent experiments on the central cathode plate and covered with a dense nickel grid. At the same time, the gap between the anode emission slit screens through which the plasma passed to the emission slit was expanded to 2.5 mm. With these modifications, the negative ion current to the collector increased to 12.5 mA, as shown in Fig. 3.

After the gas supply and discharge current had been optimized, the negative-ion collector current increased to 15 mA. Exploration of beam trajectories by means of a movable collector and a luminescent screen showed that electrons do not reach the collector. If hydrogen is fed, the ion current on the collector is primarily due to the hydrogen H^- ion beam. Heavy ions also emerge from the hydrogen discharge; they are separated from the H^- ion beam by the

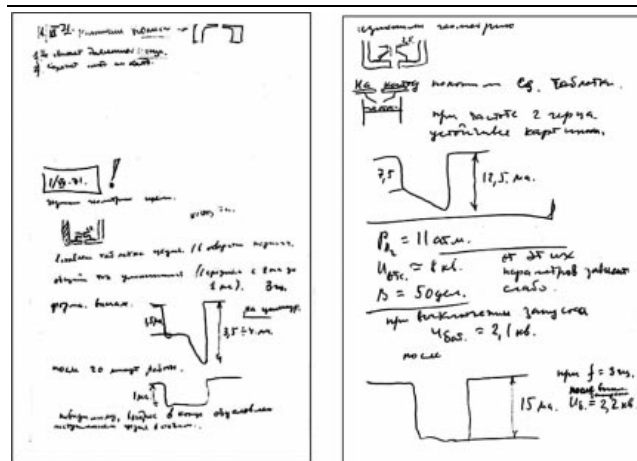**Figure 2.** Photo of the first planotron [13].

Figure 3. Pages from the laboratory log book with a description of the evolution of the intensity of the negative ion beam in adding cesium to the discharge [13].

magnetic field of the source. Observations of the discharge parameters showed that the emission of H^- ions increases with discharge voltage decreasing from $U_p = 400 - 500$ V to $U_p = 150 - 100$ V.

Thus, these pioneering experiments showed that, if cesium is added to the gas-discharge cell, the emission of H^- ions from the discharge is raised [5, 13]. A reduction in the length of the emission aperture along the magnetic field enabled better separation of the negative ion flux from the accompanying electron flux.

3. Studying emission of negative ions from discharges in hydrogen with cesium added

Adding cesium yielded a clearly pronounced increase in the emission of H^- ions from the discharge. Thus, a question arose about the mechanism that drives this increase in negative ion formation. The most probable explanation was the already familiar increase in the secondary emission of negative ions. Obtaining H^- beams with a current of up to 15 mA for the emission slot dimensions of 0.5×10 mm did not significantly disagree with the calculated possibilities for production of H^--ion beams from the gas-discharge plasma volume.

However, this possible mechanism for the production of H^- beams with a current of 15 mA from a discharge with cold electrodes provided a solution to the original problem: the development of sources that satisfy the requirements for charge-exchange injection of protons into accelerators and storage rings. In relation to this, attempts were made to optimize the generation of H^- ion beams in these sources in an empirical way. The sources were studied further using the same test-stand. The main design elements of the version of the source depicted in Fig. 1 were also preserved.

The overall schematic of power supply to the source and detection of the parameters that characterize its operations is shown in Fig. 4

The magnetic field strength B was controlled by the electromagnet current. Voltage pulses with an amplitude of up to 3 kV and duration of 1 ms that ignited and maintained the discharge were applied to the anode-cathode gap via an isolating transformer from a forming line with a wave impedance of 25 Ω by a thyratron switch. The discharge voltage U_p was monitored using a resistive voltage divider, and the discharge current I_p using a low-resistance shunt. These signals were transmitted from the high-voltage part of the circuit to oscilloscopes through isolating transformers. An extraction voltage U_0 was applied to the gas-discharge chamber casing. The total current I_0 in the extractor circuit was measured when triggered by a signal from a resistor included in the high-voltage capacitor circuitry. Hydrogen from a gas cylinder was fed to a pulsed electromagnetic valve, maintained under a high voltage, along a copper tube with an insulating section. The current pulses that open the pulsed valve were transmitted from a special circuit via an isolating transformer. Hydrogen density n_g in the gas-discharge chamber prior to discharge ignition was controlled by varying the gas cylinder pressure, the amplitude of the valve-opening current pulses, and the delay between initiation of valve-opening and voltage application to the discharge. The pulsed supply of hydrogen Q was estimated based on changes in chamber pressure, while the shape of the gas pulses was determined from signals from miniature ionization gauges.

The negative-ion beam current I^- was monitored by a movable collector, and the current density distribution J^- by small collectors located behind apertures in the main collector and a luminophore screen. At high beam intensity, the current density distribution could be visually assessed from the thermal glow of the collector. The H^- ion beam is spatially separated by the magnetic field of the source from heavy negative ions and D^- ions formed when deuterium is supplied, so the intensities of the beams could be measured
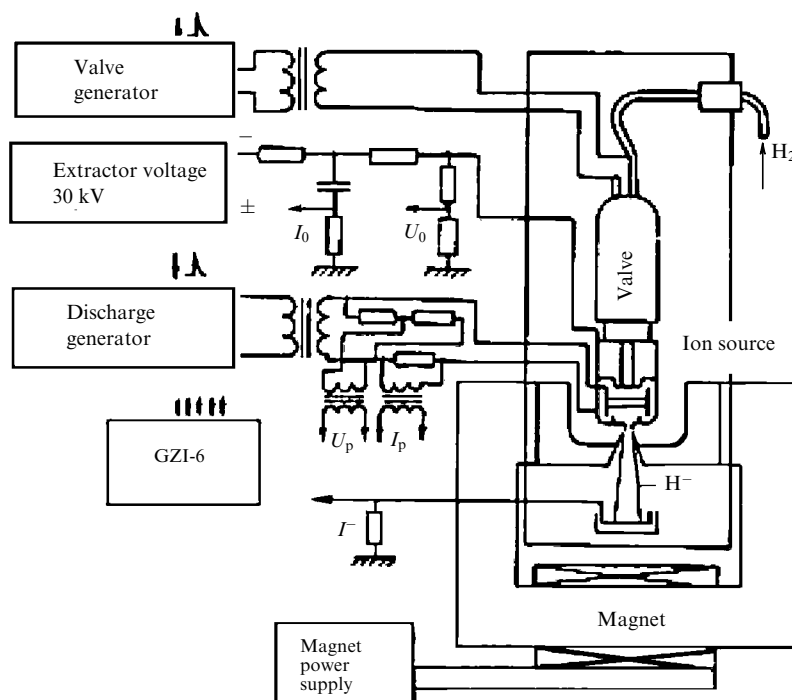

Figure 4. Schematic of an experimental setup for SPS operation and measurement of the characteristics of negative-ion production [13].

separately. The pulsed devices were controlled by a six-channel pulse delay generator GZI-6.

We managed to suppress arc discharges by making all the cathode parts and their fastenings located in the gas-discharge chamber from refractory metals with a low vapor pressure (molybdenum, tungsten, and tantalum), thoroughly cleaning their surfaces of impurities, especially from dielectric inclusions and abrasives, and carefully shielding the contacts of those parts with cathode insulators. For metal surfaces with higher vapor pressure and in the presence of gas-emitting contaminants, the arc discharge is constricted to transform into arcing in the vapors of a cathode metal or contaminants. High-current glow discharges with voltage U_p that is almost independent of the discharge current I_p are ignited under conditions that ensure efficient use of the energy of fast electrons accelerated in the near-cathode potential drop to form plasma ions. To implement these conditions, the size of the region of electron oscillations perpendicular to the magnetic field should exceed the Larmor diameter for electrons of energy U_p, and hydrogen density should be sufficient for a significant perturbation of the motion of the emitted electrons, so as to ensure irreversible capture of electrons in the oscillation region. If the magnetic field strength or the hydrogen density is insufficient to fulfill these conditions, and arc discharges are hindered, low-current glow discharges with a limited discharge current and a voltage close to the amplitude of the applied pulses are ignited.

To eliminate parasitic discharges, special electrode configurations were designed for the gas-discharge cells that form conditions for the confinement of electrons only in the main gas-discharge gap and eliminate electron oscillations in the remaining gaps. Discharges in hydrogen with cesium added burned in a more stable way if the cesium chromate/titanium tablets were placed not under a nickel grid, as was done in the first experiments, but in a cavity in the central plate of the cathode in the form of a rectangular enclosure made of 0.2–0.3-mm-thick tape or in side-shields of the same design, and with a Penning electrode configuration. Glow discharges with the minimum voltage drop, $U_p = 100$ V, that provided the largest H$^-$ ion flux were ignited in a stable way only if the temperature of the gas-discharge chamber was elevated. To ensure operability of the source at elevated temperatures, it was necessary to use high-voltage ceramic insulators, upgrade the pulsed gas valve supplying hydrogen [14], and provide more rigid mounting of all elements. These modifications made it possible to increase the pulse repetition rate to 10 Hz, accelerating the conditioning of electrodes and transition to a low-voltage glow discharge and ensuring stable operation of the source at a discharge current up to $I_p = 100$ A. The electrical strength of the high-voltage insulators and gaps was increased, as a result of which it was possible to raise the extraction voltage to 30 kV.

These improvements having been made, an H$^-$ ion beam with a current of up to $I^- = 25$ mA was extracted from gas-discharge cells with the electrode configuration shown in Fig. 1 via an emission slit with dimensions $S_e = \delta \times l = 0.5 \times 10$ mm (where δ is the slit width and l is its length). Subject to the above conditions, a variety of gas-discharge cell electrodes were produced and tested that differed in configuration, geometric dimensions, and materials. The best results were obtained for molybdenum cathodes. The configuration, geometric dimensions, and material of beam formation system electrodes were also varied.

By early 1972, H$^-$ from such sources with cesium ion beams were obtained with an intensity of up to $I^- = 75$ mA for emission slit dimensions of 0.5×10 mm, $I_{ex} = 0.2$ A; up to $I^- = 170$ mA for emission slit dimensions $S_e = 1 \times 10$ mm, with $I_{ex} = 0.5$ A; and up to $I^- = 230$ mA for emission slit dimensions $S_e = 1.5 \times 10$ mm, with $I_{ex} = 0.8$ A.

These beam currents and current emission density of up to ~ 1.5 A cm^{-2} significantly exceeded all previous achievements in the production of H$^-$ ion beams. An increase in beam intensity proportional to the increase in emission slit area created conditions to fully meet the needs of accelerator technology for H$^-$ ion beams and maintain applications that require still higher intensity of the beams. The question arose as to the mechanisms of such efficient generation of negative ion beams.

To obtain information about the location and mechanism of the formation of negative ions in these sources, dedicated experiments were performed. For a more detailed clarification of the role of cesium, an exact replica of the source shown in Fig. 1 was made from which H$^-$ ion beams were produced, if cesium was added, with an emission current density of up to 1.5 A cm^{-2} and an intensity of up to 230 mA for $S_e = 1.5 \times 10$ mm. Special precautions were taken this time that precluded even accidental contamination of the source with cesium. We studied the emission of H$^-$ ions from hydrogen discharge plasma in the cells with the planotron and the Penning geometry of the electrodes that was obtained from the planotron geometry by removing the central cathode plate. Discharges were ignited in these cells with almost identical characteristics quite similar to the discharges in the first versions of the source without a cesium feed. In gas-discharge cells with a 1-mm gap between the central cathode plate and the edges of anode emission slit screens, high-current glow discharges were ignited in a magnetic field $B = 0.12$ T and the estimated initial hydrogen gas number density $n_g = 10^{16}$ cm^{-3}. As the discharge current was increased, discharge voltage increased slightly, and decreased somewhat with increasing hydrogen supply and magnetic field strength. By varying emission slit dimensions in discharges of pure hydrogen, H$^-$ ions beams were obtained with an emission current density of up to $J^- = 200 - 270$ mA cm^{-2}. The emission current density somewhat decreased as the width of the emission slit was increased. An H$^-$ ion beam current up to 22 mA was extracted with an emission slit of dimensions $S_e = 1 \times 10$ mm, whereas H$^-$ beams with a current up to $I^- = 170$ mA were obtained from an identical source with cesium added.

On the whole, the results obtained did not contradict the idea that H$^-$ ions are generated in the volume of the hydrogen gas-discharge plasma. Since the potential to optimize conditions for the formation of H$^-$ ions in plasma sources with standard designs even in pulsed mode was limited due to the very large co-extracted electron fluxes, a significant increase in the ion current seemed reasonable without hypothesizing new mechanisms of ion generation.

However, the results of studies of H$^-$ ion emission from hydrogen-cesium discharges were completely incompatible with this mechanism, primarily because of the high density of the generated H$^-$ ion flux that was many times greater than the most optimistic estimates of the capacities to generate H$^-$ ions in the plasma volume. If deuterium was injected into these sources instead of hydrogen, D$^-$ ion beams were extracted with approximately the same intensities. A number of observed effects indicated a significant role of cathode processes in the formation of negative ions:

(1) As the gap between the central cathode plate and the emission slit increased, the maximum H^- ion current noticeably decreased, although it remained relatively large. The H^- ion current from sources with a Penning electrode configuration, with the same dimensions of the side-shields and the same discharge currents, was about half of that value.

(2) Mass spectrometry of extracted negative ion beams showed that the flux of heavy negative ions consists primarily of O^- ions. If cesium fluoride was used instead of a mixture of cesium chromate and titanium, a significant number of F^- ions were observed. The intensity of the O^- ion flux that strongly depended on the material of the central cathode plate was minimal if the cathode was made from molybdenum melted in a vacuum.

(3) The extraction of negative ions from discharges was tested with the addition of lithium, sodium, and potassium. In this case, hydrides of the corresponding metals were placed in the cavity of the cathode central plate. Vapors of these metals reduced the glow discharge voltage to $U_p = 200 - 250$ V, and the intensity of the H^- beams under comparable conditions was greater than from discharges without additives, but for K and Na it is 2–3 times less that with cesium added [15].

The complete identity of discharge characteristics in gas discharge cells with the planotron and Penning electrode configurations allowed us to hope that the major part of the discharge voltage is concentrated in a narrow near-cathode layer, as is the case in high-current Penning discharges.

4. Studying energy spectra of H^- ions from surface plasma sources

We intended to separate ions produced on the cathode by performing an energy analysis of the extracted negative ion beams. A schematic of the experimental setup is shown in Fig. 5. A source of negative ions (*2*) with pole tips (*4*) was installed in a small chamber between the poles of an electromagnet in such a way that the H^- ion beam passed into a large vacuum chamber horizontally. The heavy-ion beam was separated from the H^- ion beam in the magnetic field of the source. Part of the H^- beam passed through the entrance slit to the analyzing capacitor (*10*) at an angle of $45°$ to its plates. The ions deflected by $90°$ by the electric field of the capacitor fell on a detector (*11*) (a Faraday cup or the first dynode of a secondary-electron multiplier (SEM)) through the output slit of the analyzing capacitor. To increase the speed and

sensitivity, the signals from the Faraday cup and the SEM were transmitted by means of cathode followers.

In studying the energy spectra, H^- ions were extracted through emission slits (*7*) of width $\delta = 0.2 - 0.5$ mm and length $l = 1 - 10$ mm. Voltage sources provided long-term stability of the extraction voltage U_0 and the voltage U_{cond} on the capacitor with an accuracy of ~ 1 V at a level of 10^4 V. For accurate measurement of these voltages, digital Shch-1412 voltmeters with precision dividers were used. Rapid changes in these voltages were transmitted to oscilloscopes via capacitive dividers. The input and output slits of the analyzing capacitor were 0.05-mm wide and had sharpened edges; the distance between the slits was 20 cm. These parameters correspond to a calculated energy resolution of ~ 5 eV for the beam energy used, 10^4 eV. To quickly view the spectrum on the oscilloscope, a sawtooth sweep was added to the DC voltage across the analyzing capacitor. The beam energy spectrum could be measured at selected times of source operations within a time of 10^{-4} s. The source operated at a repetition rate of 0.1–10 Hz with full reproducibility from pulse to pulse.

Simultaneous registration with high accuracy of the accelerating voltage U_0 and the voltage across the analyzing capacitor U_{cond}, which correspond to tuning to a sharp maximum in the energy spectrum over a wide range of variation of these voltages, allowed reducing the error in determining the absolute energies of the detected ions to $\delta W < 20$ eV at a beam energy of $W \sim 10^4$ eV. The energy scale for fast scanning of the energy spectra was gauged by the shift of the spectra for small changes in the beam extraction voltage. Examples of H^- ion beam energy spectra obtained from discharges in a planotron with cesium added are shown in Fig. 6, which displays a selection of oscillograms. Two peaks separated by a dip are observed in the energy spectra of beams from the planotron. The energy width of the first peak at lower energy decreases with increasing hydrogen supply, the intensity of discharge noise being reduced. The discharges without recorded fluctuations in sources without cesium added (and in the case of Penning electrode configurations also with cesium added) were used to produce H^- ion beams with a small energy width of the first peak comparable to the resolving power of the analyzer. Multiple careful measurements of the energy corresponding to the maximum of the first peak showed that, if a negative accelerating voltage U_0 was applied to the gas discharge chamber casing, then, within the accuracy with which H^- ion energy was measured, $W_0 = eU_0^\pm \sim 20$ eV.
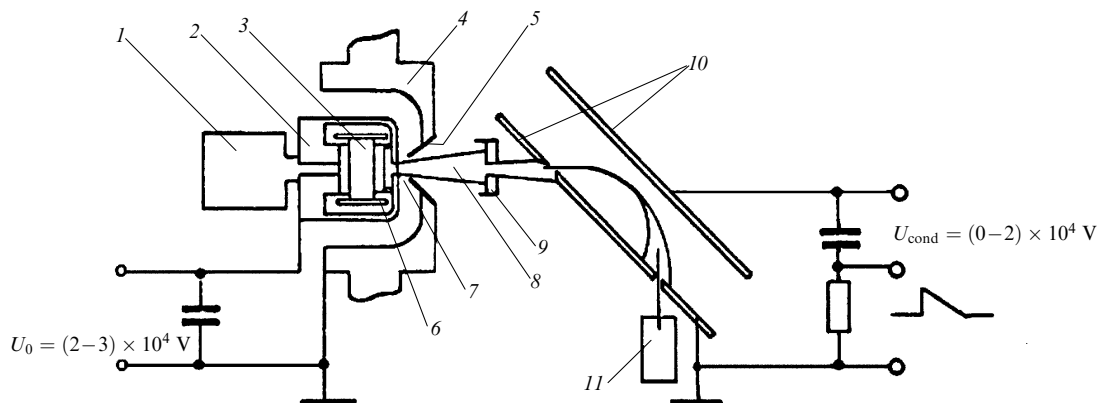

Figure 5. Setup for measuring the energy spectrum of H^- ions from planotron and Penning discharges [13] (see details in the text).
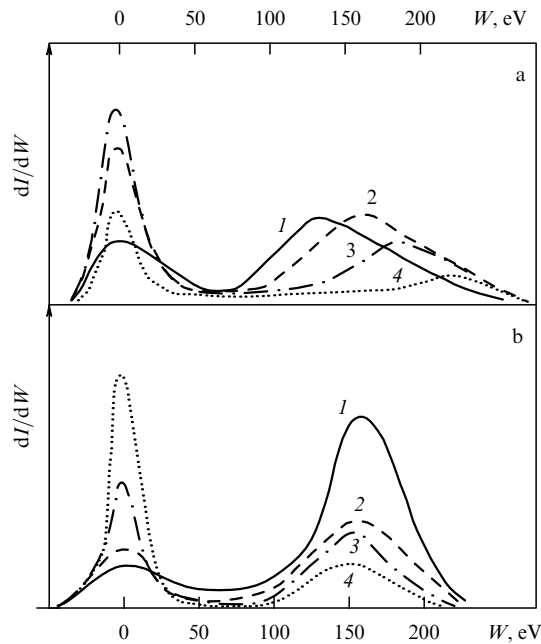
Figure 6. Energy spectra of H$^-$ ion beams extracted from discharges in cells with a planotron electrode configuration (discharge with fluctuations) [13]: (a) for various discharge voltages U_p: (*1*) 120 V, (*2*) 150 V, (*3*) 160 V, (*4*) 210 V; (b) for various hydrogen feed Q (number of molecules): (*1*) 10^{16}, (*2*) 1.2×10^{16}, (*3*) 1.7×10^{16}, (*4*) 2.2×10^{16}.

If an accelerating voltage was applied to the planotron cathode for the energy W_c that corresponds to the peak of the second maximum, a similar relation was observed; however, due to the larger peak width, the uncertainty in the energy determination was greater. The distance between the maxima, $\Delta W = W_c - W_0$, was close to or slightly greater than eU_p. This can be clearly seen in the series of oscillograms shown in Fig. 6a, for which the discharge voltage was varied by changing the cesium flow. The measurement results suggest that first-peak ions (with $\langle W \rangle = W_0$) are formed in the anodic region and in the nearly-equipotential volume formed by the anode emission slit screens near the emission slit and exit through the emission slit with low velocities. Second-peak ions are formed at the cathode bombarded by a flow of gas-discharge plasma particles due to the capture of electrons from the cathode to the electron affinity levels of sputtered and reflected particles and accelerated to the emission slit by the total discharge voltage [16, 17]. The energy width of the second peak is comparable to the distance between the maxima due to discharge voltage fluctuations and large initial velocities of the emitted H$^-$ ions that emerge as a result of momentum exchange between the particles that bombard the cathode and those of the condensed phase of the cathode and adsorbed material.

In beams obtained from discharges with cesium added in a planotron with a small gap between the cathode and anode, and with minimum hydrogen supply Q_{min}, almost all the beam ions are concentrated in the second peak near the energy W_c. If the supply of hydrogen increases, the intensity of the ion flux with $\langle W \rangle = W_c$ decreases, while the ion flux with $\langle W \rangle = W_0$ increases (Fig. 6b). These data suggest that, under the conditions of the experiment, the main component of slow ions in the anode region near the emission slit is formed due to resonant charge exchange on hydrogen atoms
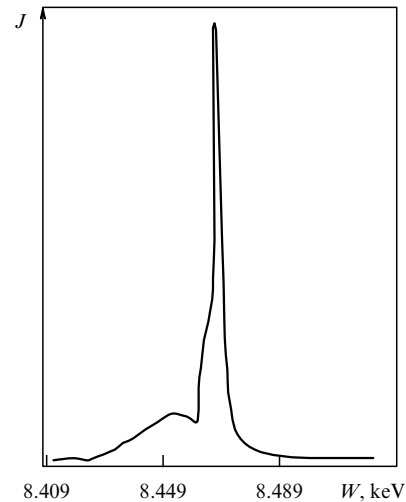

Figure 7. Energy spectrum of H$^-$ ions emitted from a Penning discharge [13].

of fast primary H$^-$ ions generated at the cathode; this process is a result of interaction of plasma particles with the surface, which features a reduced work function. In ion beams extracted from a discharge in a Penning cell, whose spectrum is shown in Fig. 7, only first-peak ions with $\langle W \rangle = W_0$ were detected.

In beams from discharges without cesium, the intensity of the second cathode peak was lower than that of the first anode peak by a factor of 10^3, even for the minimum hydrogen feed, and the distance between the peaks exceeded $eU_p = 400 - 500$ eV. If the hydrogen feed for discharges without cesium was increased even slightly, a second high-energy peak was not observed. In discharges with cesium, apparently only a small fraction of first-peak ions is produced due to usual plasma processes in the plasma volume. Under certain conditions, an appreciable contribution to the ion flux with energy $\langle W \rangle = W_0$ can come from the emission of H$^-$ ions from anode walls, anode emission slit screens, and the emission slit bombarded by fast particles formed as a result of the reflection of ions from the cathode in the form of atoms and from disintegration and charge exchange of fast negative ions in the plasma. The work function of these surfaces should decrease due to cesium adsorption, and a potential distribution that is favorable for the emission of H$^-$ ions should be created on these surfaces due to the ambipolar diffusion of the plasma. Possibly, it is this process that provides a significant emission of H$^-$ ions from discharges in cells with large distances between the cathode surfaces and the emission slit, in which only a very small fraction of ions can pass these distances without disintegration.

The first-peak ions from discharges without noise exhibit an intricate energy distribution (Fig. 7). It is possible that some part of the broadening is due to resonant charge exchange in the extracting electric field. Since field strength in the extraction gaps of these sources is high, the effective extent of the region with a high probability of charge-exchange is small, so the spectral broadening due to this effect is small despite the high density of atomic hydrogen in the extraction gap. The emergence of a small peak with an energy lower than that of the main peak by 19–20 eV is due, apparently, to a sequence of charge exchanges H$^- \rightarrow$ H$^0 \rightarrow$ H$^-$ in the extracting field. Similar transforma-

tions of the proton energy spectrum have been reported in [18] in studies of a diagnostic injector of fast hydrogen atoms.

Appreciable fluxes of H⁻ ions were detected from helium discharges with cesium added, the intensity of which increased substantially if hydrogen was injected into the gas-discharge cell between discharge pulses in the helium. An energy analysis of these fluxes showed that H⁻ ions are formed in this case only at the cathode due to electron capture by desorbed atomic hydrogen. In generating H⁻ ions in hydrogen, it is very difficult to distinguish emission due to adsorbed material sputtering from that due to the reflection of bombarding particles. Both these processes most likely make comparable contributions to negative-ion production.

The experiments considered have unambiguously shown the dominant role of the interaction between the gas-discharge plasma flow and the surfaces of electrodes with a reduced work function in the generation of intense negative ion fluxes. The planotron electrode configuration of the gas-discharge cell proved to be well suited to manifest the surface-plasma mechanism of negative-ion generation.

(1) Intense fluxes of gas-discharge plasma particles provide effective adsorption of hydrogen on the central cathode plate and efficient generation of a flux of fast sputtered and reflected hydrogen particles.

(2) Cesium is locked near the negative electrode by the discharge. Desorbed cesium ionizes and returns to the negative electrode in the form of ions. A number of features facilitate preservation of the low work function needed for the effective formation of negative ions, even under intense bombardment of the cathode by fast particles.

(3) The ability to ignite the discharge with the oscillation of electrons in the magnetic field at low gas density and with small gaps between the central cathode plate and the emission slit and the rapid acceleration of the formed negative ions to the emission slit in a narrow layer of a near-cathode voltage drop with compensation of space charge facilitate the efficient transport of generated negative ions to the beam forming system.
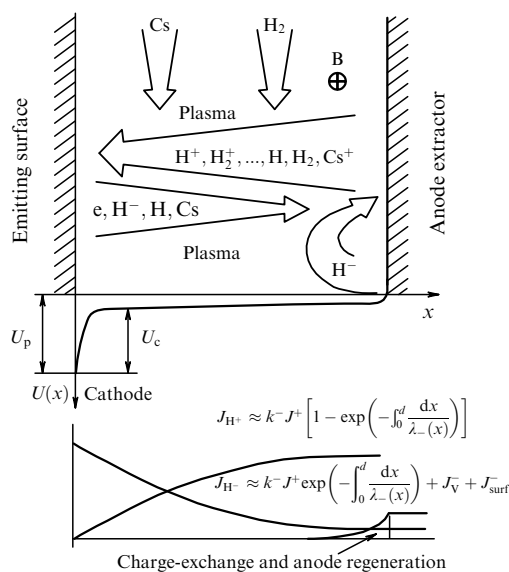

Figure 8. Diagram of the surface-plasma method for producing negative ions [13]. U_{c} is the cathode voltage drop.

(4) The orientation of the emission slit in the presence of the magnetic field, which was used in experiments, efficiently separates the negative ion flux from the electron flux and allows extraction and formation of H⁻ ion beams with an intensity by many times greater than achievable earlier.

A schematic of the surface-plasma method of negative ion production is shown in Fig. 8. The working gas and cesium are supplied to the gas discharge. The cathode is bombarded by ions and atoms of working gas and cesium. The fluxes of desorbed and reflected negative ions accelerated by the near-cathode voltage drop escape from the cathode. The negative ion flux is partially attenuated when moving through the plasma. Fast negative ions resonantly charge-exchange on the dissociated gas. The search for the dominant mechanism of negative ion formation guided the direction for further improving these sources. In subsequent versions of source designs, which could now reasonably be referred to as surface-plasma sources (SPSs), measures were taken to optimize the conditions for surface-plasma formation of negative ions and more efficient transport of the formed ions to the extraction system.

5. Advanced design options for surface plasma sources

Although it was possible in previous source designs to generate stable negative H⁻ ion beams with an intensity of up to hundreds of milliamperes with an emission current density of up to 1.5 A cm⁻², after the dominant role of the surface-plasma mechanism of negative ion formation was revealed, the shortcomings of those earlier sources became apparent. Thin-wall and almost completely thermally-insulated cathodes were easily heated by the discharge, and allowed cesium to rapidly release from tablets consisting of a cesium chromate/titanium mixture placed in internal cavities of the cathodes. At the same time, because of the low thermal inertia, the temperature regime of cesium adsorption changed very significantly during each discharge pulse, so that the optimal cesium concentration ensuring maximum efficiency of electron capture to electron affinity levels of the sputtered and reflected particles most likely failed to be established. The insufficient rigidity of cathode mounting did not allow a reduction in the gap between the cathode central plate and the anode flanges to less than 1–1.3 mm. When moving through such a plasma layer, a significant fraction of the ions formed would disintegrate. In accordance with these considerations, the central cathode plate was made in the subsequent iterations of the SPS design from a massive molybdenum bar. A more rigid fixation of the cathode provided better heat dissipation and allowed the reliable use of small gaps (as small as 0.5 mm) between the central cathode plate and the anode emission slit screens. The mounting of the source between the poles of the magnet was eased, high-voltage insulation was improved, dimensions were reduced, electrodes of the beam formation system were made more carefully, and a new small electromagnetic pulsed valve was used [14]. A schematic of this source is shown in Fig. 9.

In making the first source, special measures were taken to prevent accidental contamination of its parts by cesium. Primarily, emissions of H⁻ ions were studied with a source operating without cesium and with a massive cathode with the dimensions $4 \times 6 \times 14$ mm and a small gap of $d = 0.5$ mm between the cathode and the anode flanges near the extraction

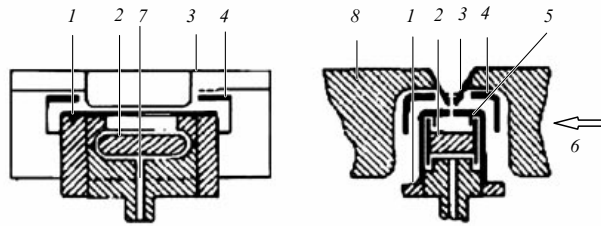**Figure 9.** Surface-plasma source with a massive cathode [13]: *1* — anode, *2* — cathode, *3* — extractor, *4* — receiver of electrons, *5* — collar, *6* — magnetic field, *7* — gas feed channel; *8* — magnetic pole.

slit. A decrease in the size of the source along the magnetic field enabled a reduction in the gap between the magnetic poles, so the magnetic field strength was sufficient to ignite the discharge in pure hydrogen at $d = 0.5$ mm.

The discharge characteristics were similar to those previously obtained. For a discharge without cesium in this source, an H^- ion beam with a current of up to 15 mA was extracted through a 0.4×5-mm emission slit, the corresponding emission current density $J^- = 0.75$ A cm^{-2} being significantly greater than the value $J^- = 270$ mA cm^{-2} obtained earlier. J^- as a function of I_p is shown in Fig. 10.

The emission current density is in this case significantly greater than the calculated capacity of volume mechanisms of negative ion formation in hydrogen plasma. If the gap increases, the maximum intensity of the extracted beam
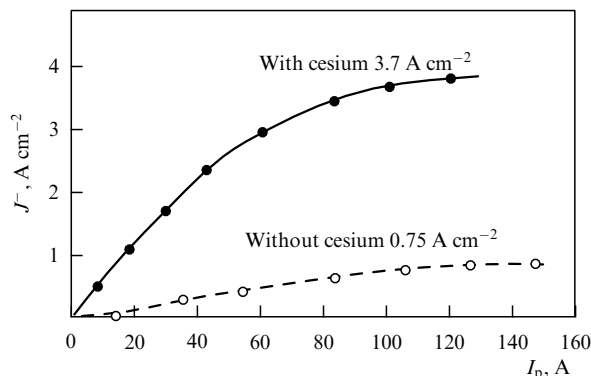

Figure 10. Emission density of H^- ion current as a function of discharge current [13].

sharply decreases. When heated to a high temperature, alkali metals apparently released from the source parts that catalyzed the surface-plasma formation of negative ions without adding cesium.

Subsequent experiments studied H^- ion emission from discharges with cesium added. Cesium was introduced, as before, into a source with dimensions of the cathode central plate of $4 \times 6 \times 14$ mm in the form of tablets containing a mixture of cesium chromate with titanium that were placed in a cavity in the cathode central plate under spot-welded cathode side-shields. The cathode was strongly heated when the discharge was ignited without cesium. However, after cesium was released and the discharge voltage reduced from $U_p = 400$ V to $U_p = 100$ V, the discharge power dissipated on the cathode decreased, and the cathode heating diminished. In nonenhanced modes, these sources operated in a quite stable way. To obtain beams with maximum intensity, careful optimization of the gas supply and the cesium release were required. The H^- ion beam intensity on the collector and the total current in the extraction gap as a function of the discharge current under optimized conditions, for a source with cathode dimensions $4 \times 6 \times 14$ mm (central cathode plate area 2.5 cm^2), and emission slits dimension of 0.4×5 mm and 1×10 mm are shown in Fig. 11.

At the initial linear part of the dependence of beam current on the discharge current, the emission current density reaches 10–12% of the discharge current density. In the saturation region of this dependence for a discharge current greater than 100 A, the emission current density could be increased to 3.7 A cm^{-2}. The intensity of the H^- ion beam increases approximately in proportion to the emission slit area. The current of accompanying electrons constitutes 13% of the negative-ion current for $S_e = 0.4 \times 5$ mm and is the same as the negative-ion current for $S_e = 1 \times 10$ mm. Space-charge effects become very significant at the achieved values of emission current density. To extract an H^- ion beam with a current of 0.3 A through an emission slit with $S_e = 1 \times 10$ mm, the extraction voltage had to be increased to 30 kV. An H^- ion beam with a current of 0.2 A for an $S_e = 1 \times 10$-mm slit was obtained at a discharge current of 50 A and a discharge voltage of 100 V. These parameters correspond to the energy cost of the H^- ion in this source $P = 25$ keV per ion at an emission density of 2 A cm^{-2}. Given that the emission aperture area is in this case 25 times smaller than that of the central plate of the cathode, and the intensity of the extracted beam increases in proportion to the emission
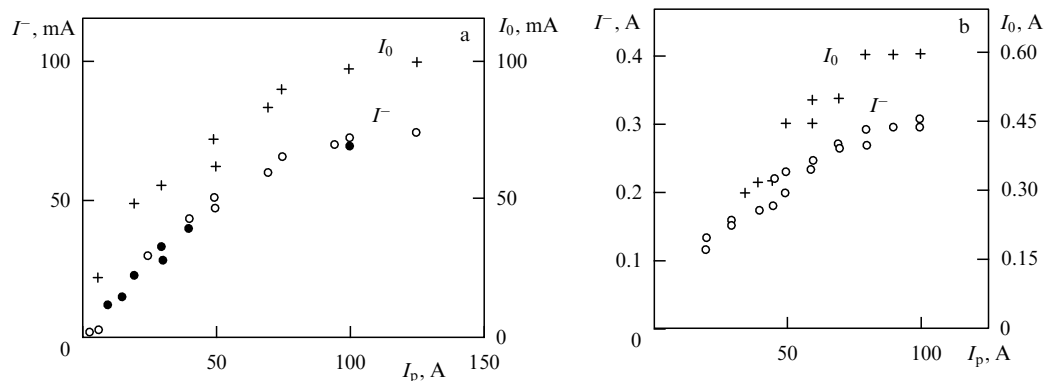

Figure 11. H^- ion beam intensity on the collector and total current in the extraction gap circuit as a function of discharge current: (a) 0.4×5-mm slit, (b) 1×10-mm slit [13].

aperture area, these results show an opportunity to enhance the efficiency of the SPS-based H^- ion generation to 1 keV per ion, a value comparable to the efficiency of the best positive-ion sources.

Thermonuclear research requires stationary and quasi-stationary beams of H^- ions. With this application in mind, the production of H^- ion beams from these sources was tested at large pulse durations. The voltage across the anode-cathode gap was applied in this case from a 50-Hz mains through a step-up transformer connected to the source by a thyristor switch. Bell-shaped pulses of discharge current with duration of up to 8 ms and amplitude of up to 50 A were obtained in this setup. The dependence of the H^- ion beam current on the discharge current remained in this regime virtually unchanged. For longer pulses, the optimal cesium feeding regime was sustained in an even more stable way than for short pulses. We investigated the emission of H^- ions from discharges in cells with a Penning electrode configuration that was obtained from the planotron configuration by removing the central cathode plate. The side shields served as the Penning cell cathodes. Removing the central massive cathode plate yielded an anode window with dimensions $S_a = 6 \times 16$ mm. Cesium tablets were located in foil boxes on the cathode side-shields. Owing to a more rigid cathode attachment, the emission of ions in forced modes could be studied.

In commonly used discharges with electrons oscillating in a magnetic field, the discharge voltage and current fluctuate with frequencies in the range of $10^5 - 10^7$ Hz, the fluctuation amplitude being up to tens of percent of the steady level. If the magnetic field decreases and gas density increases, the level of fluctuations diminishes, and for some values of these parameters vanishes, passing sometimes through a stage of coherent oscillations. The greater the magnetic field strength, the higher the gas density needed to stabilize the fluctuations. The noise level and its dependence on the magnetic field and gas density are affected by the geometric dimensions and configuration of the electrodes, discharge current, average discharge voltage, cesium concentration, and many other factors. In gas-discharge cells with small planotron cathode-anode gaps and a small transverse size of the oscillation region, a high magnetic field strength is required to ignite the discharge, and discharges without noise are obtained at a gas density so high that negative ions formed at the cathode fail to reach the emission slit without disintegration. At minimum gas density, the beam intensity and emission density are maximal, but fluctuations in the discharge greatly increase the transverse energy spread and the emittance and greatly reduce the brightness.

In the resulting cells with the Penning electrode configuration, due to the large width of the window, high-current glow discharges were ignited at low magnetic field strengths, $B > 0.03$ T. Owing to this, discharges without noise were obtained with a low hydrogen density that ensures quite normal operation of the source. Without cesium, discharges without noise were generated without any effort. If cesium was supplied to produce discharges without noise, some optimization of modes was needed. Under these conditions, H^- ion beams obtained from Penning cells with the same discharge current had a beam current approximately three times smaller than that from the planotron cells. However, the beams from discharges without noise were formed much better and featured a smaller divergence and higher collector current density, despite their lower intensity. The H^- ion current increased in proportion to the discharge current up to

150 A, so that beams with a current of up to 150 mA were extracted through a 1×10-mm emission slit, a value which is one half the maximum current from a planotron cell. If the magnetic field decreased, the current of the accompanying electrons in the extraction gap increased; however, it was successfully reduced by thickening the emission slit walls.

Assuming that only part of the cathode working area makes an effective contribution to the generation of H^- ions, we decided to investigate how ion emission depends on the anode window width. Cesium tablets were placed in this case in a thin-walled container attached to the upper anode flange that was used as an element of the anode window. This design enabled the normal release of cesium and stable burning of high-current glow discharges. With the available magnetic field strength of up to 0.3 T, high-current glow discharges were ignited steadily with a window width greater than 2.7 mm. If the field or width of the window was reduced or the flow of cesium fluctuated, high-current glow discharges transformed into high-voltage discharges with a limited current (this sometimes occurred several times during a pulse). Discharges without noise were produced with a 3×16-mm window at a field strength of $B \sim 0.08 - 0.12$ T and an acceptable hydrogen flow rate. The ratio of beam current to discharge current was only two thirds that for a planotron cell in its optimal regimes. If the discharge current was 150 A, stable and well-formed H^- ion beams with a current of up to 0.3 A were extracted through an $S_e = 1 \times 10$-mm emission slit. The discharge current density at the cathode was in this case significantly higher than the current density at the planotron cell cathode. The described results provided ways to generate intense high-quality beams with high brightness. Since brightness is the most important characteristic for the sources used in accelerator technology, we subsequently decided to use such gas-discharge cell configurations in SPSs intended for accelerators.

Thus, two areas were distinguished with slightly different tasks:

1. Production of intense beams at maximum intensity with acceptable ion-optical characteristics.

2. Production of high quality beams with high brightness at suitable intensity and efficiency.

To verify the validity of extrapolation of the identified patterns to sources with a large emission-slit area, a cathode with a central plate of dimensions $4 \times 6 \times 35$ mm and $S_e = 5$ cm^2 was placed in the same casing. A schematic drawing of this source is shown in Fig. 12. Cesium tablets were located in the cavity of the central cathode plate and a detachable upper anode flange. Discharges with the same characteristics were ignited in a stable way in this substantially enlarged cell. The emissive properties of this source, with emission slit dimensions $S_e = 0.9 \times 30$ mm, are shown in Fig. 13. Under optimum conditions, H^- ion beams with a current of up to 0.88 A, for a discharge current of 450 A, were extracted in a quite reproducible way. Thus, the possibility of obtaining beams with yet higher intensity seemed to be adequately justified.

Studying emission of H^- ions from sources with a larger emission slit width proved to be a more challenging task. As the width of a single emission slit increases, the flow of accompanying electrons increases greatly. As early as the first studies of H^- ion emission from discharges in crossed fields, we attempted to extract ions through sectioned emission slits engineered in the form of louvre grid, as is effectively done to form beams in charge-exchange sources.
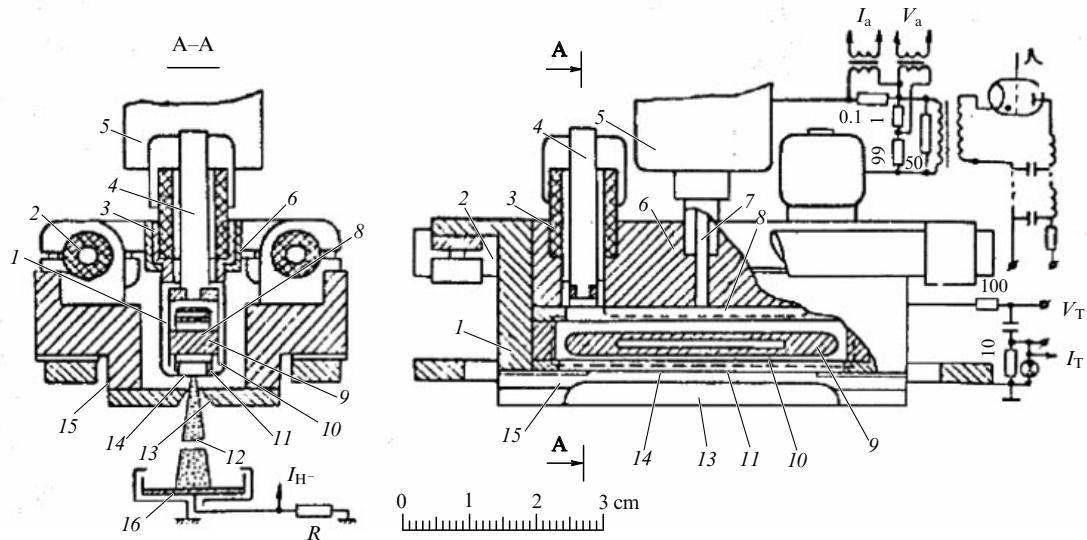
Figure 12. Schematic diagram of an SPS with a planotron gas-discharge cell configuration with a long cathode [13]: *1* — gas-discharge cell casing, *2* — high-voltage insulators, *3* — cathode insulators, *4* — cathode holders, *5* — pulsed hydrogen supply valve, *6* — anode insert, *7* — hydrogen supply channel, *8* — detachable anode flange with cavity for cesium , *9* — central cathode plate, *10* — cathode side-shields, *11* — anode flange walls, *12* — H⁻ ion beam, *13* — extractor plates, *14* — emission slit, *15* — magnet pole tips, *16* — beam collector.
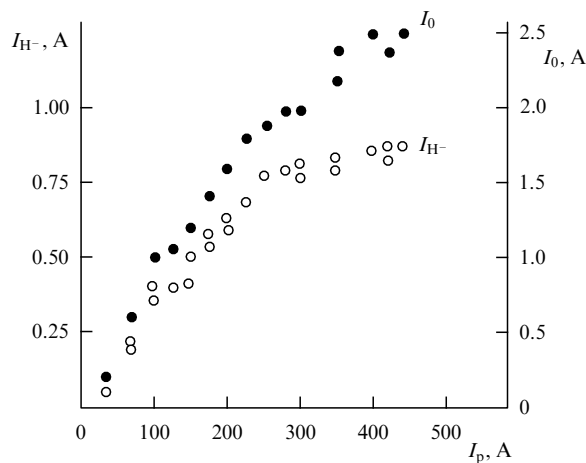

Figure 13. H⁻ ion beam collector intensity and total current in the extractor gap circuit as a function of discharge current [13].

As the width of the emission slit with a nonsectioned plasma-electrode aperture with a single-aperture extracting electrode increases, the effective length of the extraction gap increases; as a result, the extraction voltage should be significantly increased to obtain the previous density of H⁻ ion emission current. The emission aperture of the source of the previous design was blocked by a grid of strips, as a result of which the length of the obtained slits along the magnetic field was small. The main experiments were carried out with emission slit dimensions $S_e = 2.8 \times 10$ mm sectioned with a louvre grid into four identical emission slits. The cross section of the louvre grid was 0.1×0.5 mm. The molybdenum louvre grid was fixed in a mandrel at one end and could expand freely without deforming when heated.

The design of this device is shown schematically in Fig. 14. This source was studied on a new test-stand adapted for an extraction voltage of up to 70 kV. Without any structural changes whatsoever to the source design, and after extending high voltage insulators, carefully screening insulator contacts with electrodes, and thoroughly cleaning the casing of the gas discharge chamber and extraction electrodes, and with a
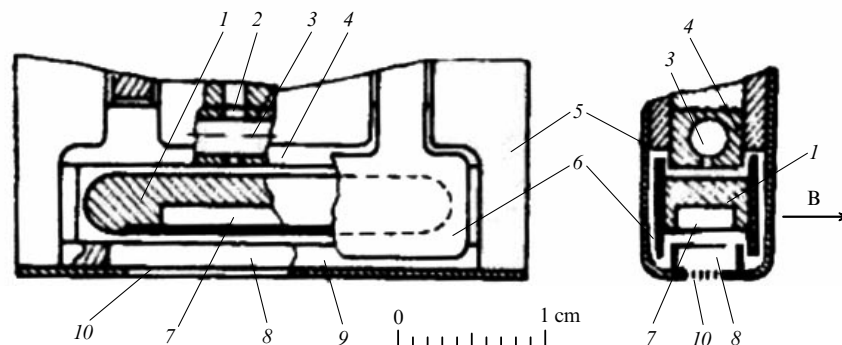

Figure 14. Schematic diagram of an SPS with a sectioned emission slit [13]: *1* — central cathode plate (CCP), *2* — hydrogen supply channel, *3* — container for cesium in the anode flange, *4* and *5* — gas-discharge chamber casing, *6* — cathode side shields, *7* — CCP cavity for cesium, *8* — expander in anode flange, *9* and *10* — sectioned emission slit.

minimum gap between the wall with the emission aperture and the extractor electrode edges of 3 mm, we were able to extract H⁻ ion beams at an extractor voltage of up to 60 kV. Stable H⁻ ion beams with an intensity of up to 0.8 A per cm of the emission slit were obtained comparatively easily. With careful optimization, beams with an intensity of about 1 A were obtained. At a collector located 10 cm away from the emission slit, the beam cross section was close to a circle 4 cm in diameter. The total current in the extractor slit exceeded the beam current by a factor of two. In this case as well, the ratio of ion current density H⁻ and discharge current density H⁻ at the cathode was, under optimal conditions, as high as $J^-/J_p = 0.12$ in the linear part of the dependence of ion current H⁻ on the discharge current. The louvre grid used endured quite steadily prolonged operation in forced modes with pulse durations of 0.8 ms and a repetition rate up to 3 Hz. The empirical optimization of the conditions under which H⁻ ions are produced in discharges with cesium added and the experience gained in handling such discharges enabled an increase in the intensity of H⁻ ion beams of up to hundreds of milliamperes at an emission current density of up to 1.5 A cm⁻². Subsequent studies, particularly exploring the energy spectra of extracted ions, which were performed in 1972, convincingly demonstrated the dominant role of the surface-plasma mechanism in formatting negative ions in the sources under investigation.

Dedicated optimization of the conditions for surface-plasma formation of negative ions and an improvement in the transport of the produced ions through the plasma allowed an increase in the emission current density of the extracted beams up to 3.7 A cm⁻². Based on this, we succeeded in creating surface-plasma sources that generate in a stable way H⁻ ion beams with a pulsed intensity of up to 1 A. Studies of these sources showed the possibility of yet further increasing the beam intensity by enlarging the emission slit area, and the conceptual possibility of reducing the cost of generating H⁻ ions in such sources to at least 10 keV per ion, a value comparable to that of obtaining positive ions in the best sources.

The realization of effective H⁻ ion generation in discharges without fluctuations in the plasma parameters established a basis for designing sources of high-quality H⁻ ion beams with high brightness. The resulting efficiency of negative ion formation and intensity of the produced beams are determined by the efficiency of production and acceleration of bombarding ions in the gas-discharge plasma, the probability of emission of negative ions from the surfaces of electrodes that are bombarded with plasma particles, the probability of disintegration of negative ions during their transport through the plasma to the forming system, and the operational efficiency of this system. The emission properties of electrode surfaces are, in turn, strongly affected by the processes that accompany the interaction of plasma with the electrodes, while the plasma properties depend on the emission properties of the electrodes.

6. Emission properties of electrodes in discharges of surface plasma sources

General concepts of mechanisms that support high-current glow discharges with oscillating electrons in a magnetic field show that, given the effective coefficient γ of secondary ion-electron emission of a cold-cathode, the electron emitted into the plasma from the cathode and accelerated to energy eU_p by

the cathode voltage drop must create, on average, in the plasma $1/\gamma$ ions that fall onto the cathode. Owing to the dependence of γ on bombarding ion energy and the dependence of the ion generation rate on electron energy, a certain value of the near-cathode potential drop U_p is set. The distribution of the potential in the plasma must provide the escape of electrons to the anode across the magnetic field, consistent with the loss of ions going to the cathode and anode. If electron diffusion is restricted by the magnetic field, the field mechanism of electron transport should prevail. The distribution of the formed potential should prevent ions from leaving to the anode and increase the efficiency of ion collection by negative-potential electrodes. If the transverse dimensions of the gas-discharge cell are small, the potential drop in the plasma should be small in comparison with the cathode drop that is concentrated in a thin near-cathode layer.

The extension of the layer depends on the ion current density on the cathode, the near-cathode potential drop, the negative ion current density, and ion mass, in accordance with the Child–Langmuir law. If the cathode is separated from the anode by a gap with insulated face ends, then, if the magnetic field is strong, the voltage drop in the plasma may exceed the near-cathode drop. Thus, the burning voltage of the discharges under study should be determined to a large extent by the emission properties of the cathode. A significant decrease in discharge voltage when cesium is added indicates a significant increase in the coefficient of secondary electron emission. The plasma density could be determined using the cathode current density; however, to estimate it, data on the coefficient of secondary emission of electrons from the cathode in SPS discharges are also needed.

Owing to the strong dependence of the discharge voltage U_p on the emission properties of the electrodes, the discharge voltage can be used as a parameter that characterizes the emission properties of the electrode. Since cells with various electrode configurations yield discharges with virtually identical characteristics, provided conditions for the efficient use of fast electron energy for ionization in plasma are maintained, it may be assumed that the same discharge voltages are obtained in various cells with similar electrode emission properties. The conditions for H⁻ ion generation are uniform across the entire surface of the central plate of the planotron cathode. While the emission current density of the extracted beam is J^-, the power spent to generate ions in the unit-area discharge region is $J_p U_p$.

The energy spent to form an H⁻ ion in the source P^- is determined by the ratio of the product of discharge current density J_p and discharge voltage U_p to the emission current density J^-:

$$P^- = \frac{J_p U_p}{J^-} = \frac{eU_p}{\varkappa} .$$

The values of $\varkappa = J^-/J_p$ that are determined from the linear parts of the dependence of I^- on I_p and correspond to various planotron discharge voltages under optimized conditions are shown in Fig. 15. As the cesium feed increases, $\varkappa$ increases from 0.01 at $U_p = 500$ V to $\varkappa = 0.1-0.12$ at $U_p = 100$ V. Concurrently, P^- decreases from 50 to 1 keV per ion. In most of the implemented SPS versions, the emission slit area S_e is smaller than the area S_c of the cathode central plate, so only a small fraction of the generated H⁻ ion flux is extracted, and the energy spent to obtain an H⁻ ion in the extracted beam proves to be factor of S_c/S_e larger.
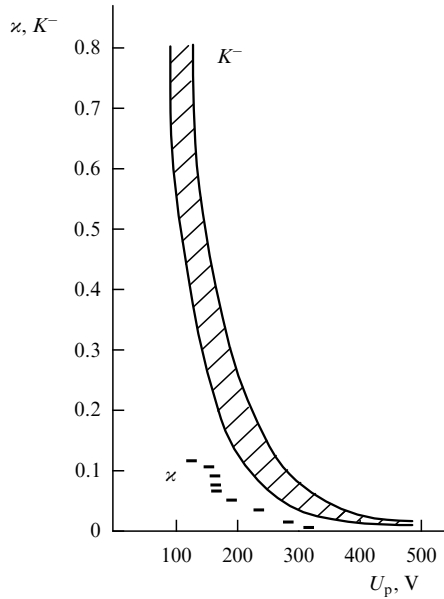
Figure 15. Ratio $\varkappa$ of the emission density of H^--ion current extracted from the discharge in planotron-geometry cells to the density of cathode discharge current, $\varkappa = J^-/J_\mathrm{p}$, and the estimated values of the coefficient of secondary emission K^- of H^- ions from the planotron cathode at various discharge voltages U_p [13].

A number of SPS designs (with closure of electron drift in one plane [19, 20], without closed electron drift [21], and with geometric focusing [21]) should allow almost complete extraction of the entire H^- ion flux that reaches the emission surface of the beam formation system, so that a decrease in the energy spent to $P^- \sim 1$ keV per ion is also possible when ions are generated by a discharge with cold electrodes. The ratio $P^- = eU_\mathrm{p}/\varkappa$ takes into account the energy spent for the emission of electrons P_e, the cost of generating positive ions P^+ and accelerating them to bombardment energy E^+, the probability of emitting H^- ions in a single bombardment event K^-, and disintegration of H^- ions during transport to the emitting surface of the beam formation system and at the beam formation stage. For plasma densities that are not too high, the probability w^- of the passage of H^- ions through the system without disintegration can be increased to close to unity, so that a general expression for the energy cost of generating H^- is

$$P^- = \frac{(P^+ + E^+)S_\mathrm{c}}{K^- w^- S_\mathrm{e}},$$

the limit of which is the relationship

$$P^-_\mathrm{min} = \frac{P^+_\mathrm{min} + E^+}{K^-},$$

which only depends on the values of K^- at the energy of the bombarding particles E^+.

If the width of the gap between the central plate of planotron cathode and the emission slit is small, the biggest fraction of the extracted flux of H^- ions consists of ions emitted from the cathode. In this case, the realized values of the coefficient of secondary emission of negative ions $K^- = J^-/J^+$ can be estimated using the known values $\varkappa = J^-/J_\mathrm{p}$ if the fraction of positive ions in the discharge

current at the cathode $J^+/J_\mathrm{p} = (1 + \gamma + K^-)^{-1}$ is determined.

The first estimates of values of the ratio J^+/J_p were obtained at the initial stage of studies of the emission of H^- ions from the discharges under consideration. The density of positive ion current to the cathode was estimated based on emission through a slit with dimensions $S_\mathrm{e} = 0.3 \times 5$ mm in the cathode of a reversed planotron. In this case, the walls of a molybdenum box served as the cathode, and a plate-like anode was located in the center, similar to the cathode of the direct planotron. Discharges in the reversed planotron were quite similar to those in the cells of other configurations. Positive-ion beams with an emission current density of up to 7 A cm^{-2} were extracted from this cell. As cesium release from tablets placed in the anode cavity increased, the ratio J_p/J^+ increased from values close to unity at $U_\mathrm{p} = 500$ V to 2–3 at $U_\mathrm{p} = 150$ V.

We attempted next [22] to estimate the coefficient of secondary emission of electrons from the cathode γ using the ratio of power released at the anode and the cathode of a cell with the Penning configuration of cooled electrodes that was used in SPSs for accelerators. We measured the average power W_c and W_a of the power carried away from the cathode and anode by cooling air. The source was operated in a pulsed mode with a pulse duration of 200 μs and repetition rate of 10–50 Hz. The release of cesium was controlled by varying the average discharge power. The air temperature at the outlet of the cooling system was monitored by thermocouples. To calibrate the system, heat-insulated calibrated electric heaters were installed in the cooling channel. The air flow was controlled by differential pressure on the cooling line. The ratios $\alpha = W_\mathrm{c}/W_\mathrm{a}$ obtained for various discharge voltages are shown in Fig. 16. As the cesium release increases, the ratio decreases from $\alpha = 6-6.5$ at $U_\mathrm{p} = 400$ V to $\alpha = 2.5$ at $U_\mathrm{p} = 100$ V.

The ratio of discharge current density to positive-ion cathode current density was directly measured in a gas-discharge cell with the Penning electrode configuration [23]. Special measures taken enabled the elimination of parasitic discharges outside the anode window. A positive-ion flux that
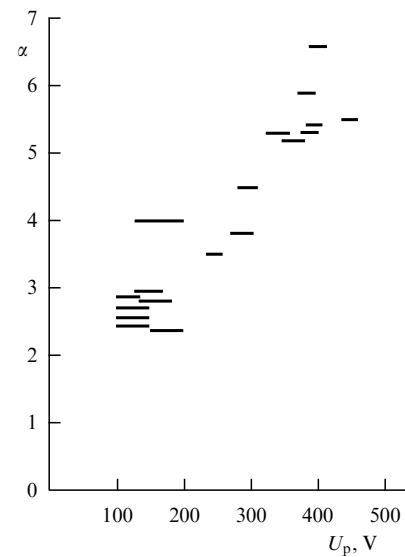

Figure 16. Ratio of the average power supplied to the cathode to that supplied to the anode of the gas-discharge cell at various discharge voltages [13].
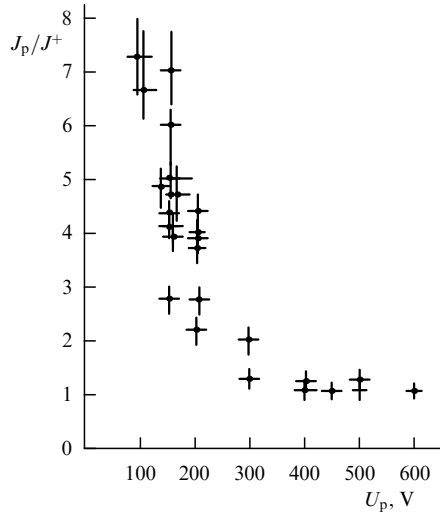

Figure 17. Ratio of the density of cathode discharge current J_p and the density of the cathode current of positive ions J^+ of a Penning cell at various discharge voltages U_p [13].

Figure 18. Oscillograms of discharge current I_p and fluxes of hydrogen from an SPS with a discharge, q_p, and without it, q_0 [13].

was accelerated in the near-cathode potential drop and emerged through a narrow slit in the cathode was recorded. Sharp-edge slits 0.01–0.05 mm wide in the molybdenum cathode were used. Slit dimensions were measured using a microscope and laser radiation diffraction. A grid with a mesh 0.2 mm in size and a transparency of 80% was placed between the slit and the collector, to which an adjustable retarding potential was applied. The volt-ampere characteristics of the collector, which were recorded automatically, showed that a nearly monochromatic flow of positive ions with an energy that is less than eU_p by 20–30 eV and an energy spread of $\sim 10-30$ eV hits the collector. The ratio of discharge current to collector ion current was monitored using an oscilloscope when the discharge was powered by half-sinusoidal voltage pulses. Measurements were carried out at discharge currents for which the near-cathode layer width was greater than the gap width. At a high discharge current, the ratio of ion current to discharge current sharply decreased, apparently due to bending of the plasma boundary and defocusing of the ion flux that entered the gap. The value of J_p/J^+ for various discharge voltages recalculated taking into account the slit size and the discharge current distribution is shown in Fig. 17. Ampules containing metallic cesium were then placed into the anode cavity, sheltered from the discharge plasma. As cesium release increased, the ratio of current densities increased from a value close to one at $U_\mathrm{p} = 600-300$ V to $J_\mathrm{p}/J^+ = 7-8$ at $U_\mathrm{p} = 100$ V.

If the emission properties of the electrodes in cells with planotron and Penning electrode configurations differ only slightly for identical discharge voltages, it follows from these data that, if cesium concentration at the electrodes increases, the coefficient of secondary emission of H$^-$ ions should increase from $K^- = 0.01$ at $U_\mathrm{p} = 500$ V to $K^- \sim 0.6-0.8$ at $U_\mathrm{p} = 100$ V (see Fig. 15.) The realized J_p/J^+ values may be used to estimate energy losses in plasma on the formation of positive ions incident on the cathode, $P^+ = eU_\mathrm{p}(J_\mathrm{p}/J^+ - 1)$. The data displayed in Fig. 15 show that, as the discharge voltage decreases, the energy cost increases from $P^+ = 0.1$ keV per ion at $U_\mathrm{p} = 300$ V to $P^+ = 0.5$ keV per ion at $U_\mathrm{p} = 100$ V. Such a strong increase in the energy cost is due to a change in the energy spectrum of plasma electrons. In
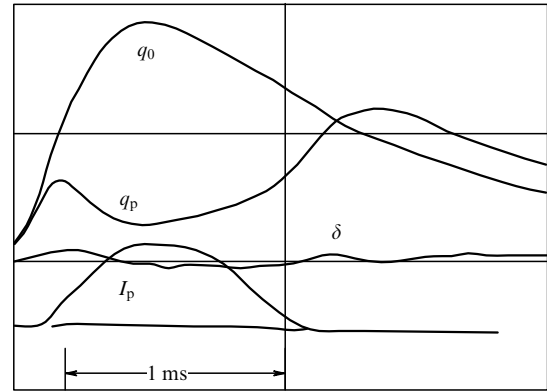
discharges with cold electrodes that are used both for plasma generation and as emitters of negative ions, it is difficult to concurrently optimize the emission properties, bombarding-particle energies, and conditions for generating bombarding particles.

In the case of independent optimization of conditions for implementation of these processes in an SPS with separated functions, one may expect to preserve the energy costs at the level $P^+_\mathrm{min} = 0.1$ keV per ion for $K^- \sim 0.8$, so it seems possible to reduce the cost of H$^-$ ion formation to $P^-_\mathrm{min} = (P^+_\mathrm{min} + E^+)/K^- = 0.25$ keV per ion. Oscillograms showing that the gas is confined by the discharge plasma are displayed in Fig. 18. The gas flow signal without discharge q_0 is more than five times greater than the gas flow signal with discharge q_p. The gas is confined by the discharge and is released when the discharge is off.

The values of magnetic field strength B and the initial gas density n_g required to ignite a discharge are consistent with estimates based on assumptions that the Larmor radius of an electron with energy $W_\mathrm{e} = eU_\mathrm{p}$ should be less than the width of the oscillation region d, while the gas density n_g should be sufficient to perturb the motion of emitted electrons. In the presence of plasma, the irreversible capture of emitted electrons into the plasma occurs due to their scattering by plasma particles, so the discharge can burn at an even lower neutral particle density. Rough estimates show that up to 5% of hydrogen supplied to the flat-cathode planotron discharge cell is converted into an H$^-$ ion beam.

It can be hoped that the initial hydrogen density in the gas-discharge cell in the SPS with separated functions and with geometric focusing during plasma generation in discharges with thermal cathodes can be reduced to the values used in positive ion sources, thereby significantly improving the gas efficiency of SPSs.

7. Cesium in surface plasma sources

The decrease in the work function of electrodes in an SPS, which has a decisive influence on the efficiency of negative ion formation, is provided by adsorption of cesium fed into the gas-discharge cell.

Cesium, the heaviest of the stable alkaline elements, features the minimum work function $\varphi = 2.14$ eV. Metals and semiconductors partially coated with cesium exhibit an even lower work function. Cesium reacts with many elements. Pure cesium melts at 28.45 °C and its boiling point is 671 °C.

The patterns of cesium adsorption-desorption and its release through the emission slit determine the generation of negative ions and the feasibility of practical applications of SPS. Data on the effect of cesium on the work function of refractory metals are systematized in reviews on thermionic converters [24, 25]. The work function φ of refractory metals decreases in the case of cesium adsorption almost linearly from $\varphi = 4-5$ eV to the minimal value $\varphi_{min} = 1.5-1.6$ eV if the cesium surface concentration is $N_{opt} = (2-4) \times 10^{14}$ cm^{-2}, and then increases to 2.14 eV for $N > (5-6) \times 10^{14}$ cm^{-2}. The work function of fluorinated or oxidized surfaces can decrease to $\varphi_{min} = 1.1-1.2$ eV for $N = (1-2) \times 10^{14}$ cm^{-2}, and, if hydrogen is adsorbed, it diminishes to 1.5 eV (Fig. 19). The work function of a thick layer of cesium with adsorbed hydrogen is considerably higher than that of a thick layer of cesium on pure tungsten [26].

To maintain the optimal surface concentration of cesium on the electrodes, it is necessary to compensate for desorption of cesium from the surface. At low electrode temperature T, the cesium flux from the volume that compensates thermal desorption is rather small. If T increases, the thermal desorption rate and the required compensating flow increase in proportion to $\exp(-l/T)$, where l is the energy of cesium desorption from optimal coatings. For optimum cesium concentration on molybdenum, $l = 2$ eV, and the heat of cesium desorption from a pure molybdenum surface is $l = 3$ eV. The dependence of l_0 and l^+ on the surface concentration of cesium on tungsten is given in [24, 25]. At $T = 600$ K, the cesium flux density $q = 3 \times 10^{14}$ cm^{-2} s^{-1} is needed to compensate for thermal desorption, which is provided at the volume density $N_V = 5 \times 10^{10}$ cm^{-3}, a value close to the density of saturated cesium vapor at $T_{Cs} \sim T/2 = 300$ K. Note that, if cesium is adsorbed on oxidized surfaces, the desorption heat is higher, and the surface concentration of the optimal coating is smaller, which should lead to a decrease in the equilibrium density of the cesium flux that maintains the optimal concentration of cesium on the surface.
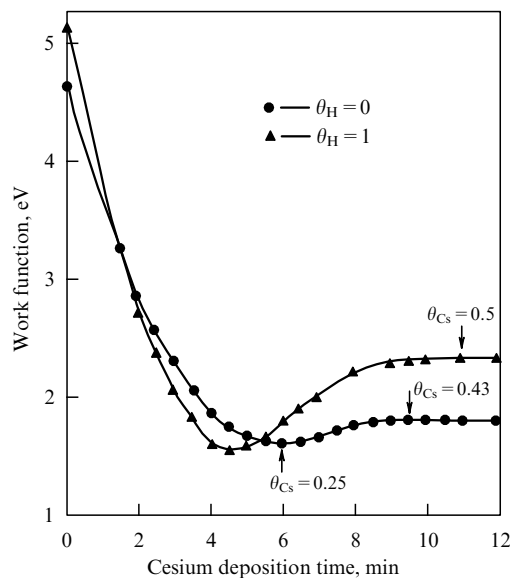

Figure 19. Work function of a pure tungsten surface and a surface containing adsorbed hydrogen as a function of surface cesium concentration [26]. θ_{Cs} and θ_H are the surface concentration of cesium and hydrogen in monolayer units, respectively.

In the SPS, the cesium adsorption–desorption kinetics on electrodes bombarded by a fast-particle flux from the discharge plasma is complicated by sputtering, pulsed overheating of the surface, ionization, and other factors. If the power density per electrode during time t from the beginning of the discharge pulse is P/S_c, the temperature T of the electrode surface will increase by $\Delta T = 2P(t)^{1/2}/S_c^{1/2}(\pi \lambda c \rho)^{1/2}$, where λ is the thermal conductivity factor, ρ is the density, and c is the heat capacity. For molybdenum, the coefficient $\varepsilon = (\lambda c \rho)^{1/2} = 1.5$ J cm^{-2} deg^{-1} s$^{1/2}$. If $P/S_c = 10^4$ W cm^{-2}, the temperature of a thick molybdenum planotron cathode increases by $\Delta T \sim 100$ K within $t \sim 10^{-3}$ s. For a cathode with $T \sim 10^3$ K, the thermal desorption flux from the optimal coating can increase due to such pulsed overheating by a factor of $\exp(l_0 \Delta T/T^2) = 5-10$ (here, l_0 is the cesium desorption energy).

Cesium is desorbed during a discharge pulse from the surface due to sputtering of fast particles from the discharge. The cathode is bombarded by H$^+$, H$_2^+$, H$_3^+$, and Cs$^+$ ions, and fast atoms, while the anode is bombarded by H$^+$, H$_2^+$, H$_3^+$, Cs$^+$, H$^-$, and fast atoms. A hydrogen particle with the energy eU_p can transfer energy $W_{max} = 4M_H eU_p/M_{Cs}$ to an adsorbed cesium atom. Under discharge conditions $U_p = 150-200$ V, $M_H = 1-3$ and $W_{max} = 4-18$ eV. Since $W_{max} > l_0$, the cesium atom can be knocked off the surface. However, the coefficient of such sputtering is small due to the narrow range of impact parameters for which the momentum transferred to the cesium particle is sufficient to overcome the potential barrier. If the density of the fast particle flux to the cathode is $\sim 10^2$ A cm^{-2}, the cesium lifetime on the cathode that is determined by sputtering by fast particles should be $\sim 10^{-4}$ s. Several factors facilitate maintaining optimal cesium concentration on the cathode. In high-current discharges, cesium atoms desorbed from the cathode surface should rapidly become ionized in plasma and rapidly return to the cathode by the electric field of the discharge.

To study the behavior of cesium in a gas-discharge chamber, the yield of ions and cesium atoms that escaped through the planotron emission slit and the yield of cesium ions through an aperture in the cathode of the Penning-geometry source were explored.

Various ways are used in the SPS to supply cesium to the discharge: from tablets made of cesium chromate with titanium that are placed in discharge-heated electrodes of the gas-discharge cell and from independently heated containers with cesium, cesium cartridges, or cesium-bismuth alloys. To stabilize the release of cesium, a filter made of molybdenum wires was inserted into the outlet tube of the container. The yield of cesium from a container with metallic cesium was measured as a function of container temperature. If Cs$_2$CrO$_4$ + Ti tablets are heated, cesium is released due to its reduction by titanium: 4Cs$_2$CrO$_4$+ 5Ti $\rightarrow$ 8Cs + 5TiO + 2CrO$_3$ [27]. A tablet that weighs 10 mg contains 1 mg of extractable cesium. The measurements have shown that the yield of cesium depends on the specific batch of tablets and the time interval during which they are used.

More detailed information on fluxes of neutral cesium was obtained using a surface-ionization detector of cesium atoms. An ionizing tungsten hotplate ($T \sim 1500$ K) heated by a tantalum heating coil was set at an angle of $45°-60°$ to the flow of atoms from the emission slit. The ions produced as a result of surface ionization were accelerated and formed into a beam using a 2-kV voltage applied between the plate and the ionizer casing. The ion beam was analyzed using a magnetic

mass spectrometer with $B < 0.25$ T, $R = 15$ cm and recorded by a Faraday cup collector. The efficiency of the detection of the cesium exiting the source was determined on the basis of the cesium flux from a heated container installed instead of the source. The measurements showed that the collector recorded 0.2% of the flux of cesium exiting the source. Information on the density of cesium ions in the cathode and anode regions was obtained by direct extraction of cesium ions from these regions by a 10-kV voltage that was followed by an analysis made using a magnetic mass spectrometer. In the same way, fluxes of H^+, H_2^+, and H_3^+ light ions were measured.

Figure 20 shows a typical oscillogram of the current of cesium ions from the mass-spectrometer collector [13]. One can see that cesium atoms leave the source primarily after the discharge pulse ends. Cesium release during the pulse is small, since cesium is highly ionized, and the extraction voltage blocks the escape of cesium ions. It has been established that the time of delay between the beginning of the signal and the discharge pulse end depends linearly on the distance between the source and the ionizer. The velocity of cesium atoms determined in this way corresponds to a temperature of 10^3 K. The dependence of the pulsed signals of cesium ions from the detector at various temperatures of the discharge chamber temperature was studied in [28]. The temperature was changed by varying the discharge repetition rate at a fixed discharge current. As the temperature of the source gas-discharge chamber increases, the pulsed release of cesium increases in a quadratic manner as a result of an approximately linear increase in the amplitude and duration of the pulsed cesium release (determined at the 1/e level). The signal amplitude is almost independent of the pulse duration at a fixed average power deposited into the discharge. The repetition rate was varied in inverse proportion to the discharge pulse duration. The amplitude and duration of the signal grow if hydrogen is added.

The quasi-stationary component of the Cs atom flux observed in intervals between discharges depends only on the average power invested in the discharge. The density of cesium ion current at the Penning cell cathode increases with
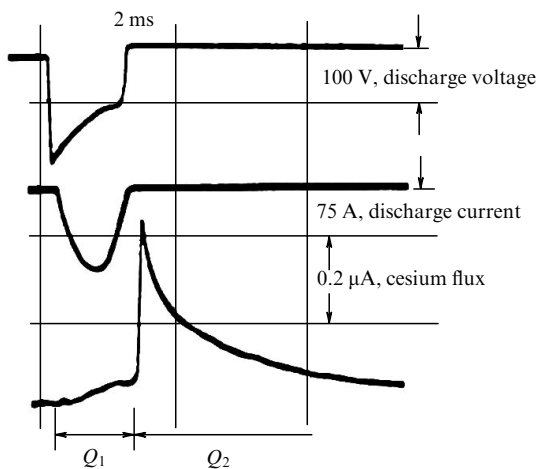

2 ms

100 V, discharge voltage

75 A, discharge current

0.2 μA, cesium flux

Q_1 Q_2

Figure 20. Characteristic oscillogram of cesium ion current from a mass-spectrometer collector that shows how cesium ion flux from the source varies with time at a high (~ 1000 K) temperature of the planotron cathode, along with the oscillograms of discharge current I_p and discharge voltage U_p [13].

discharge current and weakly depends on the temperature of the gas-discharge chamber. The main process in cesium desorption from the electrode surface during the discharge pulse is sputtering, as evidenced by the significant (compared with relative thermal desorption) cesium current density at the cathode and the growth of flux density with discharge current density J_p. The cesium flux density through the emission slit being less than the flux density at the cathode by a factor $\sim 5 \times 10^2$ indicates that the cesium desorbed from the anode is rapidly ionized in the discharge plasma and transported to the cathode by the electric field, while the cesium desorbed from the cathode returns after ionization to the cathode. The cesium ions accelerated in the near-cathode layer can sputter cesium from the surface, as a result of which the integral coefficient of cesium scattering by the surface increases.

The coefficient of scattering of cesium ions with an energy of $\sim 100 - 200$ eV by the pure surface of molybdenum is known to be $K_S = 0.6$. The coefficient of knockout K_S from a coating with $\theta = 0.3 - 0.6$ estimated for the hard-sphere model is $K_S = 0.2 - 0.3$. As a result, we have for the integral cesium scattering coefficient $K_S = 0.8 - 0.9$, i.e., a Cs particle knocked out by a hydrogen particle makes 5–10 oscillations near the cathode. If the flux density of fast hydrogen particles is $J^+ = 10^{20}$ cm^{-2} s^{-1} ($I_p = 100$ A), the density of cesium ion flux at the cathode is $J_{Cs} = J + K_H (1 - K_S)^{-1} = 10^{18}$ cm^{-2} s^{-1} (K_H is the coefficient of sputtering of cesium by hydrogen particles), in agreement with the measured value of J_{Cs}. Measurements of the flux of H^+, H_2^+, and H_3^+ light ions showed that the number of protons, i.e., the degree of hydrogen dissociation, increases rapidly with increasing discharge current. Therefore, at low discharge currents, when the molecular ions H_2^+ and H_3^+ prevail in the ion current to the cathode, the cesium ion flux density to the cathode is high due to the large coefficient of cesium sputtering by molecular ions. The surface concentration of cesium on the cathode increases toward the end of the discharge pulse, which is confirmed in experiment by an increase in the density of cesium ion flux through a hole in the cathode and a decrease in the discharge voltage. The average lifetime of cesium on the cathode surface is $\tau \sim N/J_{Cs} \sim 10^{-4}$ s (N is the surface cesium concentration on the cathode), a value that is much greater than the time during which cesium remains in the volume, $\tau_i \sim 10^{-7}$ s, the time of cesium atom ionization in the near-cathode plasma with a density of 10^{14} cm^{-3}, and the average electron energy of 10 eV. Thus, the total amount of cesium present in the plasma is small: $N_V \sim J_{Cs} S_c \tau_i \sim 10^{11}$ particles cm^{-2} (cathode area $S_c = 2$ cm^2).

In the SPS where cesium is released due to the heating of electrodes by the discharge, the supply of cesium to the cell is automatically boosted if the electrode temperature increases, so the efficient generation of negative ions is maintained when the electrode temperature T varies over a wide range. Adjustable cooling of electrodes allows a significant reduction in the consumption of cesium; however, an adjustable cesium supply should also be used. Measurements of the cesium flux through the emission slit showed that the cesium flux from the SPS during the discharge is very small, but increases sharply after the discharge terminates (see Fig. 20). Release of cesium during a discharge is hindered by its rapid ionization in the discharge. The extraction voltage prevents the release of cesium ions through the emission gap. Since the field mechanism of electron transport across the magnetic

field prevails, cesium ions should be efficiently transported to electrodes having a negative potential. The cesium desorbed from these electrodes is quickly ionized and returns.

The drastic increase in the cesium flux after the end of the discharge pulse is due to the unimpeded release of neutral cesium that appears in the volume after the discharge ends, while a gradual decrease in the flux is due to adsorption of cesium on cooled electrodes. The increase in the surface concentration of cesium results in an increase in the coefficient of secondary emission and a decrease in the discharge voltage. A reduction in sputtering and thermal desorption due to the decreased energy of bombarding particles facilitates a further increase in the surface concentration of cesium. If the cesium flux is sufficiently large, the discharge voltage demonstrates an avalanching decrease due to this feedback to the minimum value $U_p = 100$ V, which corresponds to the maximum coefficient of secondary electron emission at the minimum work function. The decrease in binding energy with increasing concentration limits the accumulation of excess cesium. These considerations show that a concentration of cesium, somewhat greater than the optimal value, should be stable. It may be hoped that, in the case of cooled electrodes, the optimal cesium concentration will also be maintained in high-current steady discharges.

In an SPS for accelerators [29], H$^-$ ion beams with a current of 0.1 A, pulse repetition rate of 100 Hz, and pulse duration of 0.25 ms are generated at an average cesium consumption rate of $\langle q \rangle \sim 10^{-3}$ g h^{-1} $\sim 10^{15}$ particles s^{-1}. The average H$^-$ ion flux exceeds in these sources the average flux of cesium atoms by a factor of 10, while the ratio of intensities during the discharge burning is over $10^3 - 10^4$. The H$^-$ ions proved to be efficiently generated in the SPS with low requirements for a vacuum. Actually, cesium is accumulated under typical SPS conditions on the walls of the gas-discharge cell in the form of compounds: oxides, hydrides, etc., so the cesium flux from the source in the interval between discharge pulses also proves to be small at the elevated temperatures of the gas-discharge cell casing.

Changes in the properties of surfaces under SPS conditions have been studied very poorly to date. Persistence of the high efficiency of H$^-$ ion production under bombardment of a surface by intense particle fluxes from a plasma is a nontrivial and very important phenomenon. It may be hoped that an in-depth study of this issue will help enhance the efficiency of H$^-$ ion production and increase the stability and durability of SPSs. The best results have been obtained so far with emitting electrodes made of molybdenum. Tungsten seemed to be preferable due a number of features; however, numerous experiments failed to confirm this assumption. Due to looser atomic packing, reflection of hydrogen particles from tungsten is presumably limited by deeper penetration into the lattice. A molybdenum emitter yields smaller fluxes of heavy ions, primarily O$^-$. Since molybdenum atoms are lighter than cesium atoms, the coefficient of reflection of accelerated cesium ions from molybdenum is much less than that from other refractory metals. This effect facilitates maintenance of optimal cesium concentration on the molybdenum emitter under intense bombardment, since cesium ionized in the discharge and accelerated to the emitter is better captured by the molybdenum surface. The efflux of cesium through the emission aperture can be reduced by means of ionizing cesium between pulses by a weak discharge if cesium is excited by resonance laser radiation [30].

Lowering the work function by implanting cesium ions into copper and molybdenum has been tested in [31]. Cesium ions were implanted at an energy of 10–20 keV to a close of $10^{18} - 10^{19}$ cm^{-3}. The samples were heated afterwards to 900 °C. The estimated work function is $\varphi \sim 1.9$ eV. The secondary emission of negative ions from residual gas increased as a result of such treatment by a factor of 7 to 8.

8. Surface plasma sources of H$^-$ ions for accelerators

H$^-$ ion beams with parameters suitable for a number of applications were obtained yet at an early stage of SPS studies. In relation to this, development of SPS designs adapted for specific applications commenced. We first turned to solving the original problem: creating a source for accelerators that would be capable of ensuring efficient applications of charge-exchange techniques in accelerator technology and, first and foremost, charge-exchange injection of protons into accelerators and storage rings. The choice of source parameters was guided by the needs of the linear accelerator of the meson factory at the Institute of Nuclear Research of the USSR Academy of Sciences (Troitsk) [32, 33]: a pulse intensity of 100 mA, pulse duration of 0.1 ms at a repetition rate of up to 100 Hz, and normalized emittance of < 0.5 mm mrad. Production from a planotron-cell SPS of H$^-$ ion beams with the emission current density of several amperes per cm^2 ensured the required beam brightness.

However, experience in handling ion sources gained at the Institute of Nuclear Physics showed that fluctuations in the parameters of the emitting plasma cause crucial deterioration of the ion-optical characteristics of intense beams. Discharges without fluctuations (plasma noise) were only obtained in SPSs with the planotron electrode configuration at high hydrogen density, when the efficiency of H$^-$ ion generation substantially decreases to become comparable to the efficiency of beam production from an SPS with the Penning electrode configuration, in which discharges without fluctuations are obtained more easily. Beam brightness is the most important quality characteristic of ion sources employed in accelerator technology. Since we had hoped that some reduction in efficiency and emission density would be more than compensated by an increase in brightness due to the elimination of plasma fluctuations, a decision was made to generate H$^-$ ions in a cell with the Penning configuration of electrodes [34].

The beams were extracted in the already implemented SPS versions through a long narrow emission slit oriented across the magnetic field in order to improve filtering of accompanying electrons from the ion flux. The ion-optical system of the source forms a beam with two planes of symmetry: quasi-parallel cross-section boundaries along the slit and with wedge-shaped cross-section boundaries in the perpendicular direction. In relation to this, a problem arises as to how such a wedge-shaped beam may be transformed into a quasi-parallel and symmetric beam. A solution to this problem is to additionally form the beam by means of the focusing field of a segment of a bending magnet with a nonuniform field. By placing the source in such a way that the emission slit is located in the median plane of the magnet, the wedge beam can be converted into a beam with any configuration of 4D phase volume by the appropriate choice of the decay index n and the azimuthal extent of the magnet ϕ. We initially chose the simplest version of beam formation: conversion of the
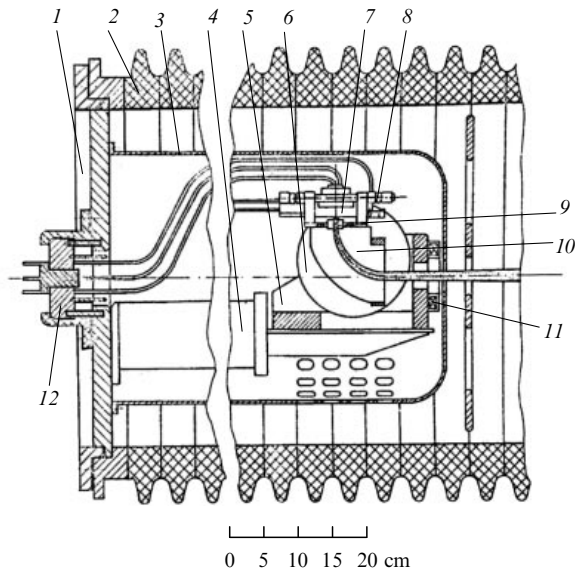
Figure 21. Diagram of SPS matching with a pre-injector accelerating tube [13]: *1* — high-voltage accelerating-tube flange, *2* — tube insulators, *3* — external shield of the source, *4* — support rod, *5* — source electromagnet yoke, *6* — sealed electromagnet coils, *7* — source gas-discharge chamber, *8* — high-voltage source insulators, *9* — extractor plates, *10* — deflecting focusing magnet poles, *11* — Rogowski coil, *12* — bushing insulators.

wedge beam into a beam that is quasi-parallel in both transverse directions due to bending by $\phi = 90°$ in a magnet with the field index along radius $n = 1$.

The scheme proposed for matching the source with the accelerator system of a standard linear accelerator pre-injector is shown in Fig. 21 [13].

The beam has to pass through the bending magnet in a compensated state and, after exiting the magnet yoke and the screen, be dragged by a strong electric field of the first accelerating gap and the contracted field of the main gap of

the accelerator tube. By varying the voltage ratio at these gaps it is possible to adjust the focal length of the system within some limits. If a more significant change in optical character-istics is needed, other configurations of bending magnets may be used.

9. Design of surface plasma source for accelerators

By the time work on a source for accelerators began (1972), the production of H⁻ ion beams with an intensity of 100 mA had no longer been a problem. The only remaining problem was to form symmetric quasi-parallel beams with high brightness and ensure long-term operation of the sources at high repetition rates. In developing designs of a source for accelerators, the expertise gained in handling SPSs was employed. The first designs of the source were tested on the same test-stand with an electromagnet, a chamber pumped by an N-5 diffusion pump, and a power system that was employed earlier.

The design of one of the first versions of an SPS for accelerators described in [32] is shown in Fig. 22. Poles of the bending magnet (*14*) with pole tips (*3*) that form a field in the gas-discharge cell region were installed between the magnetic-circuit poles that pass through the vacuum-chamber wall. The gas discharge chamber was installed between the pole tips on high-voltage ceramic insulators (*5*). The walls of a slot in a massive molybdenum rod (*9*) served as the cathodes of the Penning gas-discharge cell. The anode window consisted of parts (*11*) and (*12*) of the casing of chamber (*4*) and anode insert (*6*) made of stainless steel. The discharge cell preserved in this electrode configuration the basic features of previous SPS designs, but the cathode mount (*8*) was made stronger and adapted to forced cathode cooling. Hydrogen volumes were fed through a channel by a small electromagnetic valve (*10*) [14] designed by that time that could operate at a frequency of up to hundreds of hertz. The source could operate using a cesium supply from an anode insert (*11*) due
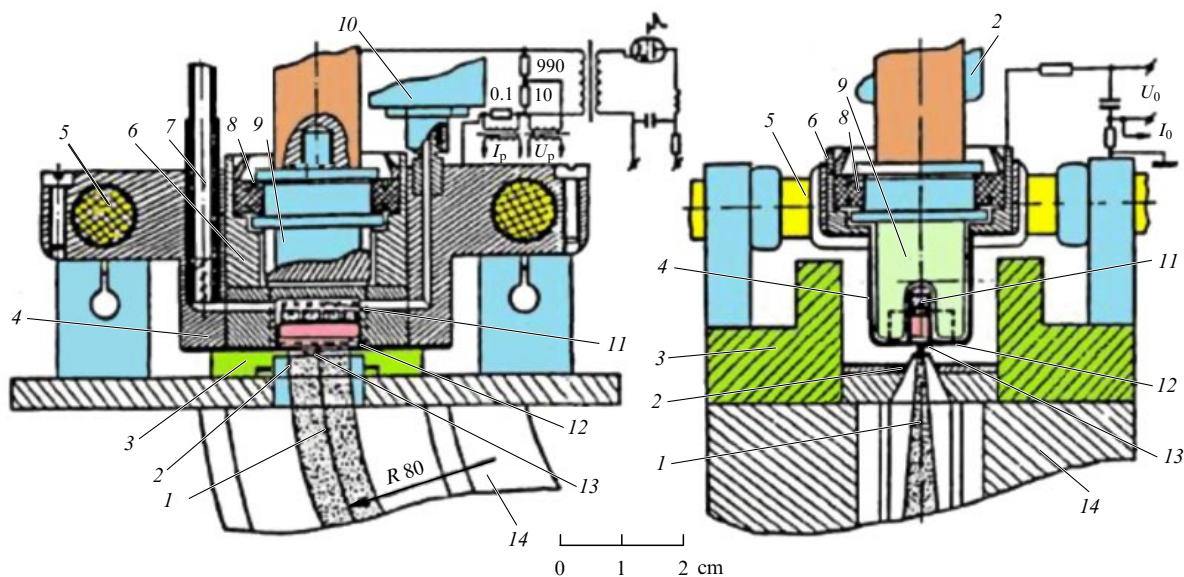

Figure 22. (Color online.) Schematic of an SPS for H⁻ ions with the Penning configuration of gas-discharge cell electrodes [13]: *1* — H⁻ ion beam, *2* — extractor electrodes, *3* — magnet pole tips, *4* — gas discharge chamber casing, *5* — high-voltage insulators, *6* — anode insert, *7* — heated container for cesium, *8* — cathode insulator, *9* — cathode, *10* — pulsed valve, *11* — anode insert with a container for cesium, *12* — anode protrusion wall, *13* — emission slit, *14* — bending magnet.
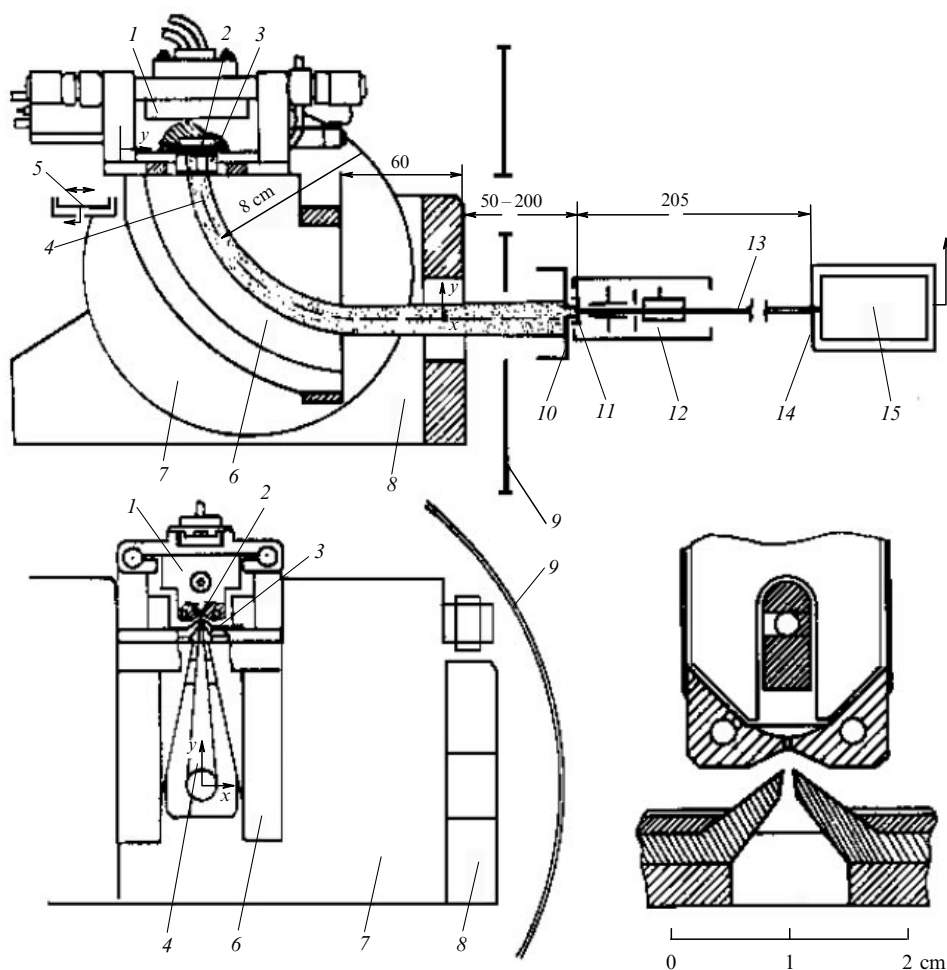
Figure 23. General layout of an SPS for accelerators and a system for recording the distribution of H$^-$ ions over transverse velocities in the focused beam [13]: *1*— SPS gas discharge chamber, *2*— emission slit, *3*— extractor electrodes, *4*— H$^-$ ion beam, *5*— movable collector, *6*— pole of bending focusing magnet, *7*— sealed electromagnet coils, *8*— magnetic circuit, *9*— source screen, *10*— collector, *11*— minor collector, *12*— ion beamlet scanning system, *13*— ion beamlet in the drift space, *14*— SEM screen with analyzing aperture, *15*— SEM.

to discharge heating of tablets placed in it that contained a mixture of cesium chromate and titanium or a cesium supply from a container (*7*) with independent heating. An H$^-$ ion beam (*1*) exited the gas-discharge chamber through the emission slit (*13*) with dimensions of 0.5×10 mm oriented across the magnetic field. The extraction field was concentrated in a 1.5-mm-long gap between the wall of the gas-discharge chamber with an emission slit and grounded extraction electrode (*2*).

The configuration of the emission slit walls and the design of the beam formation system were varied many times, until eventually we selected a simple two-electrode formation system. The distance between the cathodes was varied from 4 to 12 mm, and the transverse vertical dimension of the anode window from 3 to 8 mm. If the size of the gas-discharge cell is increased, the ratio of beam current to discharge current decreases, and if the anode window decreases, a larger initial hydrogen density and higher magnetic field strength are needed to ignite the discharge. For design reasons, the distance between the cathodes was chosen to be 5 mm and the anode window dimensions 3×15 mm. The characteristics of discharges in the source were almost identical with those of previous discharges. We soon managed to obtain symmetric beams with a current of ~ 0.1 A at the output of

the bending magnet. Estimated ion-optical divergence characteristics of thin beamlets cut from the beam by small holes in the collector showed that the requirements for emittance were more than sufficient, provided there were no discharge fluctuations; if discharge fluctuations occur, the ion-optical characteristics significantly deteriorate.

This version of the SPS without forced cooling could operate at a repetition rate of up to 17 Hz with a pulse duration of 0.6 ms. At frequencies of 50 and 100 Hz, it could continuously operate for no more than a few minutes due to overheating. The pumping rate provided by an N-5 diffusion pump with a liquid-nitrogen freezing trap was sufficient for the source operation at a frequency of up to 100 Hz. In-depth studies performed enabled the SPS design to be perfected to a state that maintained long-term operation with the desired beam parameters. The general layout of one of the latest versions of an SPS for accelerators is shown in Fig. 23. The source is adapted to be installed in the acceleration tube of the pre-injector according to the matching scheme shown in Fig. 21.

A magnetic field is excited by coils (*7*) placed in air-tight casings made of stainless steel and cooled with water. The bending magnetic field with a field index along radius $n \sim 1$ is formed by poles (*6*). The magnetic flux closes on parts of the
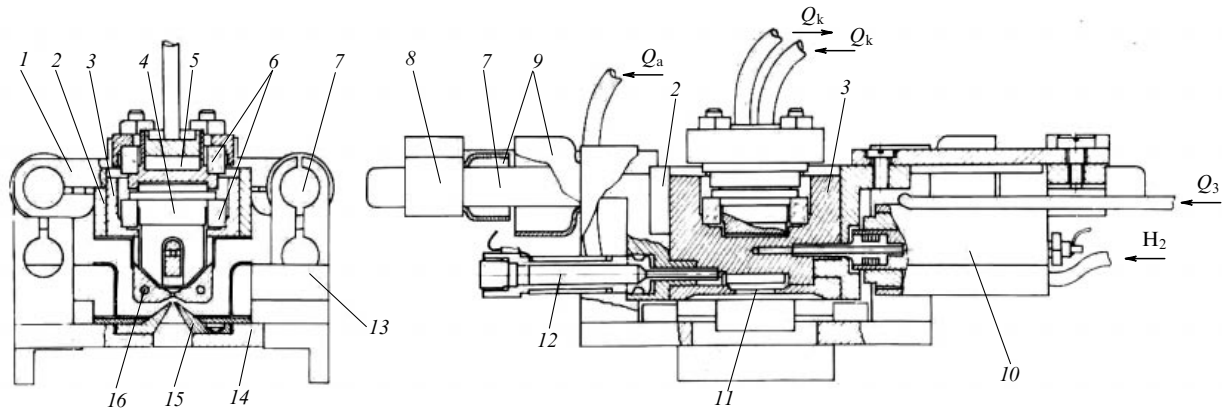
Figure 24. Schematic of an SPS with a Penning discharge of H⁻ ions for accelerators [13]: *1* and *8* — support plates, *2* — gas discharge chamber casing, *3* — anode insert, *4* — cathode, *5* — cathode cooler, *6* — cathode insulators, *7* — high-voltage insulators, *9* — screen, *10* — hydrogen feed valve, *11* — emission slit, *12* — heated container with cesium, *13* — magnet pole tips, *14* — base, *15* — extractor electrodes, *16* — cooling channel for anode wall with emission slit.

magnetic circuit (*8*) that also performs as a magnetic shield. The design of the gas discharge chamber (*1*) and elements of the beam-forming system (*2*) and (*3*) are shown in more detail in Fig. 24. This version of the source basically does not differ from the first one (see Fig. 22); however, differences in the design are rather significant [27]. Thin-walled parts that melted during long-term operation in forced modes were removed from the gas-discharge cell. A photo of this source is shown in Fig. 25.

Previous studies have shown that, to increase the efficiency of formation of H⁻ ions, it is of primary importance to optimize the emission properties of the emission-slit electrode. In this connection, the cathode is intensively cooled by a water flow, and to control cooling of the anode electrode with the emission slit, a controlled air flow is passed through channels (*16*). Cesium is fed from a heated container (*12*) with cesium tablets. The volume of the gas-discharge cell and the supply channels is minimized as much as possible, so that the time constant for the hydrogen portion to flow out through the emission slit with dimensions of 0.5×10 mm was reduced to 1 ms. The leading edge of the hydrogen density pulse in the cell is about 0.2–0.3 ms. Pulsed extraction voltage $U_0 = -30$ kV is applied to the casing of the gas discharge chamber; this voltage ensures the formation and primary acceleration of the H⁻ ion beam.

Figure 25. (Color online.) Photo of a Penning-discharge SPS. The cathode and anode inserts are seen [13].

The requirements discovered in all previous SPS studies have been consistently taken into account in this design. These improvements in the source and the development of systems that ensure its operation enabled us to achieve the following performance characteristics maintained during an extended period of source operation: pulse intensity of the formed beam of up to $I^- = 100 - 150$ mA for an emission slit with dimensions of 0.5×10 mm, pulse duration of 0.25 ms with a repetition frequency of up to 100 Hz, H⁻ ion energy of up to 25 keV, hydrogen consumption of ~ 1 cm³ Torr per pulse, and cesium consumption of ~ 0.1 g for 100 hours of operation. Operation of this source at a pulse repetition rate of 400 Hz has been tested. The oscillograms illustrating the operation of this source with corresponding power supply systems are shown in Fig. 26. The current of H⁻ ions after the bending magnet is as high as 150 mA.

10. Development of surface plasma sources at foreign research centers

Beginning in 1974, Soviet researchers were allowed to communicate with foreign colleagues (although not everything was allowed to be published). Contacts with the Brookhaven National Laboratory (BNL) group (T Sluyters and K Prelec) facilitated the development of the SPS at BNL. This group received a specimen of a planotron SPS, on the basis of which magnetron and Penning SPSs have been developed at BNL [35–37].

A schematic of the BNL duoplasmatron with tubular discharge developed at BNL is shown in Fig. 27. It was possible to extract from that duoplasmatron — after adding cesium — up to 60 mA of H⁻ ions, but with a total extractor current of 1.2 A at a discharge current of 150 A and discharge voltage of 80 V applied in 1-ms pulses. A group of H⁻ ions produced on the central rod via the surface plasma mechanism is observed in the energy spectrum of the ions. Up to 0.9 A of H⁻ ions were extracted from the magnetron SPS-planotron with an extraction circuit current of up to 2 A, discharge current of 260 A, and discharge voltage of 150 V applied in 10-ms pulses. Up to 0.32 A of H⁻ ions were extracted from the Penning-discharge SPS with a total extractor current of 0.55 A, discharge current of 80 A, and discharge voltage of 220 V applied as 4-ms pulses.
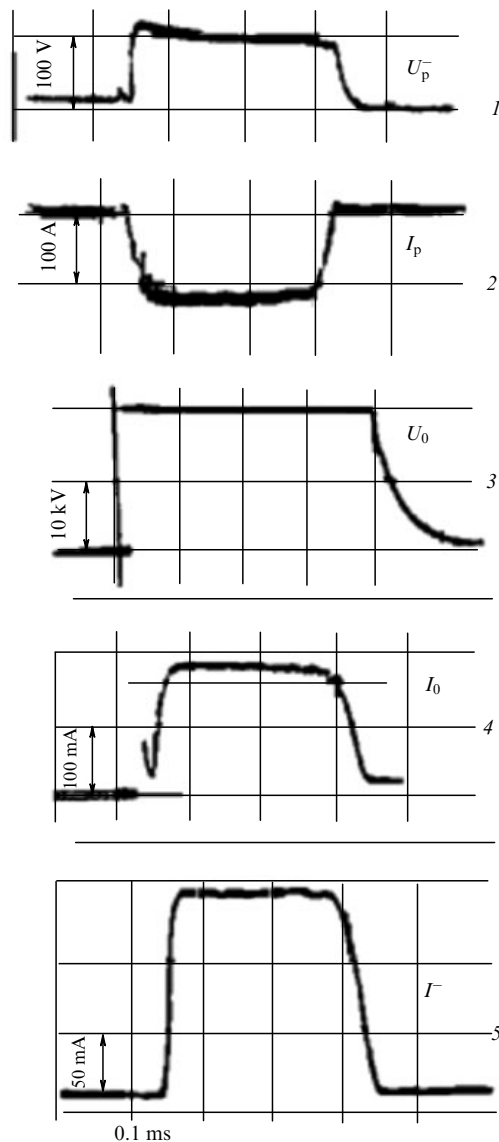
Figure 26. Oscillograms characterizing SPS operation for accelerators in a noise-free mode [13]: *1* — discharge voltage, *2* — discharge current, *3* — extraction voltage, *4* — extraction current, *5* — H$^-$ ion beam current after analyzer.

Up to 0.14 A of D$^-$ ions were extracted from a deuterium discharge with a total extractor current of 0.4 A, discharge current of 40 A, and discharge voltage of 420 V applied in 4-ms pulses. After geometric focusing had been invented at the Institute of Nuclear Physics [21], an SPS with geometric focusing was developed at BNL [38, 39]. A schematic of the asymmetric magnetron (planotron) SPS is shown in Fig. 27b. The groove curvature radius is 3.7 mm.

The H$^-$ ion current as a function of the discharge current for an asymmetric magnetron (*1*), regular magnetron with a cylindrical groove (*2*), and planar cathode magnetron (*3*) is shown in Fig. 28. The energy used to generate H$^-$ ions decreased in the asymmetric magnetron from 33 keV per ion for a flat-cathode magnetron to 8 keV per ion (in the semiplanotron SPS, the energy cost reduced to 2 keV per ion, while gas efficiency increased to 30%). A multi-slit magnetron SPS with geometric focusing for continuous operation, which was developed at BNL on the basis of a Novosibirsk prototype, is shown in Fig. 29.

A magnetron was proposed at BNL with discharge plasma generation with a hollow cathode and an independent emitter of negative ions with geometric focusing, the design developed on the basis of the Novosibirsk prototype.

In 1976, BNL sold a prototype of a planotron-type SPS for 40,000 USD to the Fermi National Accelerator Laboratory (Fermilab, USA) (see Fig. 30).

Based on this prototype SPS, C Schmidt developed a design of the planotron (magnetron), shown in Fig. 31 [40–42]. The magnetron cathode is made of molybdenum, the casing is the anode made of stainless steel, and the ceramics are a machined MACOR material. Cesium is supplied from a heated metal container with an ampoule of metallic cesium inside. A 90° bending magnet with field index of ~ 1 is used for one-dimensional beam focusing, as was done in the Novosibirsk SPS with the Penning discharge. Alignment of the H$^-$ beam with the accelerating tube at the Fermilab pre-injector is shown in Fig. 32. This SPS provided all the needs of the Fermilab accelerator facility for 35 years, and enabled developing SPSs for other laboratories. A semi-cylindrical groove was made in 1986 in its cathode [43], an improvement that allowed a reduction in the discharge current from 150 A to 35 A, with a corresponding increase in the continuous operation time. Fermilab supplied magnetrons to the Argonne National
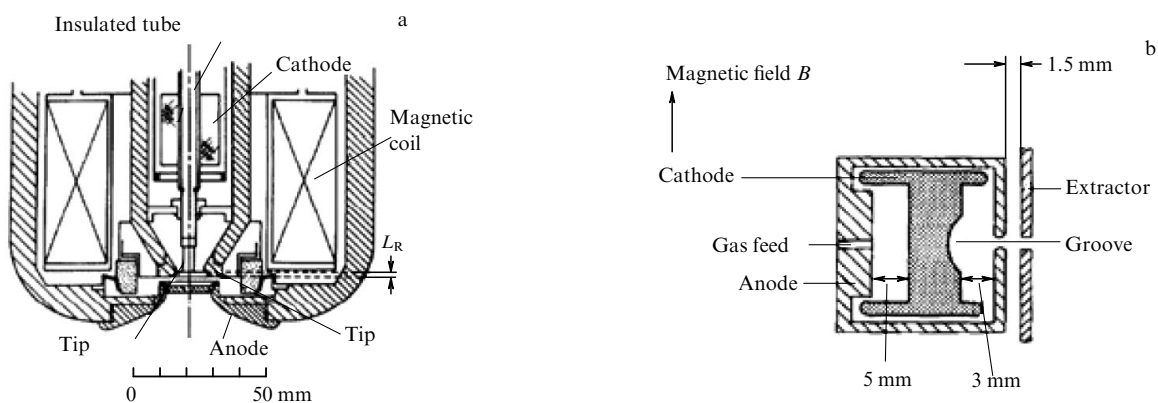

Figure 27. (a) BNL duoplasmatron SPS with tubular discharge [32]. (b) SPS asymmetric magnetron (planotron) setup. Cathode groove curvature radius is 3.7 mm [36].
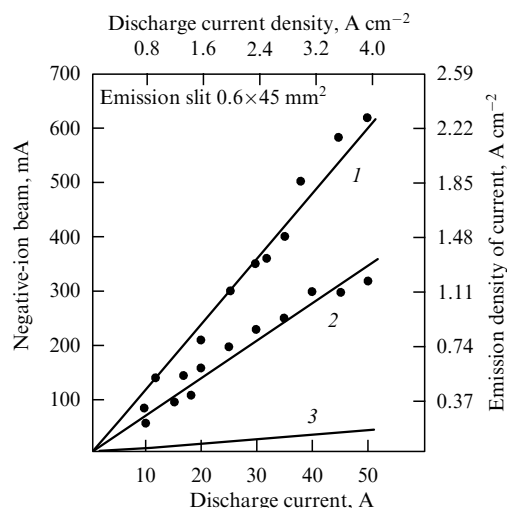
Figure 28. H$^-$ ion current as a function of discharge current in an asymmetric magnetron (*1*), a regular magnetron with a cylindrical groove (*2*), and a flat-cathode magnetron (*3*) [36].
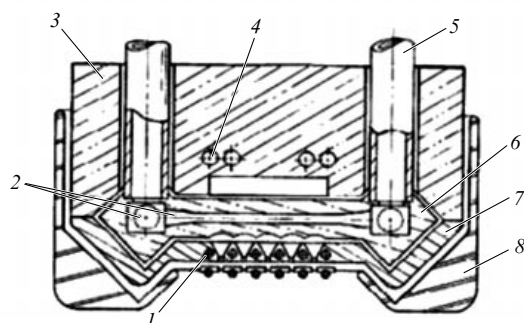

Figure 29. Multi-slit magnetron with geometric focusing designed for continuous-mode operation [37]: *1* — anode cooling channels, *2* — cathode cooling, *3* — anode, *4* — anode cooling channels; *5* — cathode holders, *6* — cathode, *7* — anode, *8* — extractor.

Figure 30. Prototype planotron-type SPS sold by BNL to Fermilab.

Figure 31. SPS magnetron developed at Fermilab [40].

Laboratory (ANL, USA) [44], BNL [45], DESY (Germany) [46], and the Chinese synchrotron [40].

Following the Novosibirsk advancement [21], in switching to an RFQ injector, BNL began using a magnetron cathode modification with a 3D spherical focusing to a cylindrical emission aperture 2.8 mm in diameter [47]. An H$^-$ current of 120 mA was obtained at a discharge current of

Figure 32. Matching of an H$^-$ beam to an accelerating tube in the Fermilab pre-injector.

14 A and discharge voltage of 130 V. The source lifetime at a duty cycle of 0.5% was 8 months (3 A h). When the Fermilab injector was re-designed using a radio-frequency quadrupole (RFQ), it was also switched to spherical focusing similar to that at BNL [48].

10.1 Development of Penning-discharge surface plasma sources at Los Alamos National Laboratory

Los Alamos National Laboratory (LANL, USA) began developing in 1972 a negative ion source for their LINAC (LINear ACcelerator) [49]. Only 2.5 mA of H⁻ ions could be obtained from the charge-exchange source. After the parameters obtained using a Penning-discharge SPS were published [29], LANL decided to reproduce these results. Ronald Reagan announced in 1983 the Strategic Defense Initiative (Star Wars) program. A Star Wars element-to-be was beams of high-energy neutrals in space that should be obtained from high-quality beams of negative ions [50–52].

Paul Allison, a Los Alamos researcher, who spoke Russian, traveled with his wife in 1976 from Japan along the trans-Siberian railway to Novosibirsk. He spent about a month in Novosibirsk, where he was allowed to familiarize himself with our SPS studies.

After returning to Los Alamos, Allison received a $ 50-million grant to reproduce the 'Dudnikov-type source' and to accelerate H⁻ ions [53, 54]. The Los Alamos's version of the Penning discharge SPS source is shown in Fig. 33. The measured emittance values in the Penning-discharge SPS (PD SPS) and the asymmetric magnetron (AM) are shown in Fig. 34 [55]. The transverse ion temperature in the PD SPS
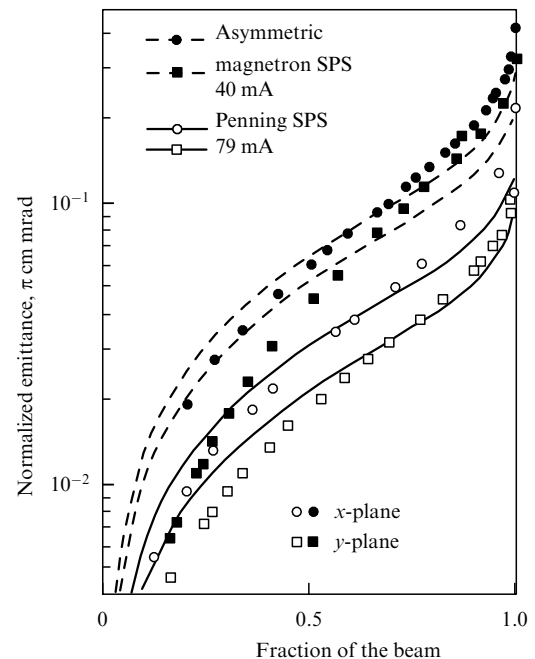

Figure 34. Measured emittance values for a Penning-discharge SPS and asymmetric magnetron [55].

with a current of 79 mA is 5 eV along the slit and 840 eV across the slit. The transverse ion temperature in the AM SPS [421] with a current of 40 mA is 22 eV along the slit and 5650 eV across the slit. The PD SPS brightness is an order of magnitude higher than that of the AM SPS.

The high transverse temperature of ions (across the emission gap) is associated with heating of the 'overcooled' ions due to expansion of the ion beam in this direction and insufficient resolving power of the emittance meter. An injector developed at LANL that preserves high beam brightness [56] is shown in Fig. 35. A strong electric field picks up the beam after a minimal drift. The angular spread of the beam from the Penning-discharge SPS is shown in Fig. 36. The effective transverse ion temperature along the slit is ~ 3 eV, while across the slit it is 24 eV. Near the SPS, the emittances are 0.27π mm mrad along the slit and 0.04π mm mrad across the slit. After the accelerator column, emittances are 0.23π mm mrad along the slit and 0.19π mm mrad across the slit.

The LANL group measured the ion temperature of the beam extracted from a PD SPS whose size was eight times larger than the original size [57]. The measurements were based on the angular broadening of the beam extracted through a narrow slit (along the slit). In the case of a low discharge current (up to 2 A), the transverse ion temperature was 0.1–0.3 eV, while at a high discharge current (of up to 400 A), the transverse ion temperature was 0.7–1.3 eV. This is the basis for obtaining beams with very high brightness.

A similarity theory for such discharges was developed [58]. SPS specimens were engineered that were 4 (×4) and 8 (×8) times larger than the original Dudnikov source. These specimens are shown in Fig. 37. A study of the emittances of H⁻ ion beams from a ×4 PD SPS has been reported in [59]. With an emission aperture of 5.4 mm in diameter for a 100-mA beam from a discharge with a noise of > 20%, an emittance of 0.22π mm mrad was obtained, while for a 67-mA
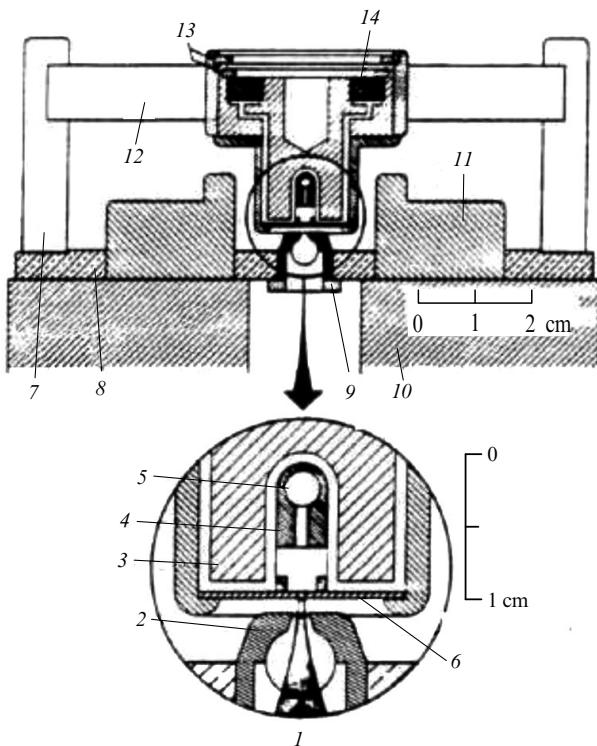

Figure 33. Los Alamos version of a Penning-discharge SPS (Dudnikov source) [53, 54]: *1* — ion beam, *2* — extractor, *3* — cathode, *4* — anode, *5* — hydrogen and cesium supply channel, *6* — plasma electrode with an emission slit, *7* — source holder, *8* — base, *9* — extractor, *10* — bending magnet, *11* — source magnet, *12* — high-voltage insulator, *13* — pressure ring, *14* — cathode insulator.
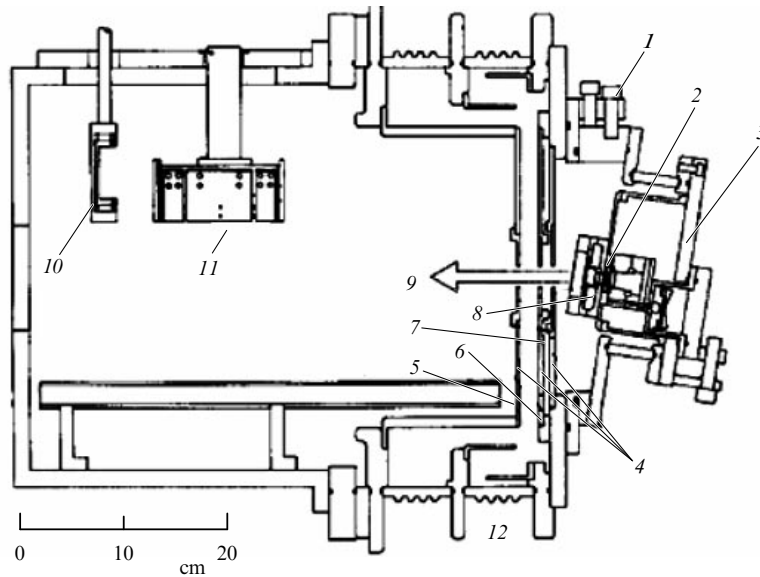
Figure 35. LANL injector that maintains high beam brightness [56]: *1* — source position adjustment; *2* — SPS (−100 kV), *3* — source flange (−100 kV), *4* — evacuation hole, *5* — grounded electrode, *6* — suppressor (−90 kV), *7* — intermediate electrode, *8* — extracting electrode (−78 kV), *9* — H$^-$ ion beam, *10* — Faraday cup, *11* — emittance measuring device, *12* — high-voltage insulator.
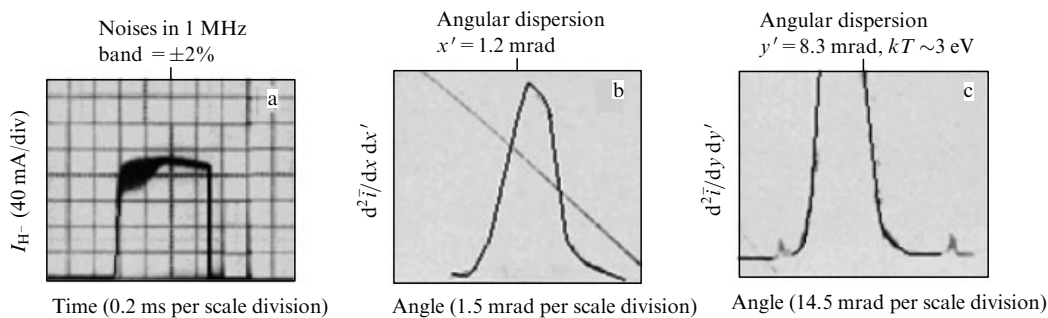

Figure 36. Angular dispersion of beam from a Penning-discharge SPS [56].

beam from a discharge with a noise of $< 1\%$, the emittance was 0.11π mm mrad. The potential of this quiescent beam was measured in [60] at various densities of gaseous Xe and various ion trap potentials. The beam potential becomes positive if the Xe density is greater than 5×10^{11} cm^{-3} and sharply increases to 10 V if the Xe density is more than 7×10^{11} cm^{-3}. The emittance of the beam after transport over 36 cm increased from 0.12 to 0.23π mm mrad if the Xe density decreased from 2.2×10^{12} cm^{-3} to 0. In this case, up to 1.5×10^{12} cm^{-3} of hydrogen remains in the operating SPS. A noise-free discharge was obtained by adding a small admixture of nitrogen [61, 62]. The oscillograms of the current of the H$^-$ ion beam from Penning discharges with and without nitrogen added are shown in Fig. 38. If even a small amount of nitrogen (1%) is added, discharge becomes noise-free, and emittance is reduced. The H$^-$ ion beam was extracted from a ×4 SPS with an emission slit of 2.8×11 mm with a current of 250 mA and emittances of 0.15–0.29π mm mrad.

Suppressing the noise by adding a heavy gas is explained by an ignition/burning diagram for a discharge in crossed fields in the coordinates n (gas density) and B (magnetic field) [63] displayed in Fig. 39a. The discharge burns if the gas density is higher than a certain value and the magnetic field is stronger than $B_{\min}$.

If the gas density is above critical value n^*, discharge becomes noise-free. The transverse mobility of electrons in the magnetic field is given by the formula $\mu = ev/m\,(v^2 + \omega^2)$, where v is the electron scattering frequency and ω is the Larmor frequency of the electrons (Fig. 39b). If $\omega < v$, excitation of noise increases the collision frequency and reduces mobility, factors that hinder the transmission of current. If $\omega > v$, the emergence of noise increases mobility, a factor that facilitates the current flow, and instability develops. Therefore, a small addition of a heavy gas increases the electron collision frequency and suppresses discharge noise, thus increasing the beam brightness. An attempt to obtain an intense H$^-$ ion beam from a Dudnikov-type source with lanthanum-hexaboride cathodes without cesium has been reported in [64]. A beam of H$^-$ ions with an emission current density of up to 350 mA cm^{-2} (from a 0.5×10-mm emission slit) at a discharge current of 55 A without cesium was obtained, a value that is much less than the value 0.75 A cm^{-2} obtained from discharges without cesium in [16, 17].

10.2 Development of Penning-discharge surface plasma sources at Rutherford–Appleton Laboratory

The development of a Penning-discharge SPS commenced in 1979 at the UK-based Rutherford–Appleton Laboratory

Figure 37. Scaled-up Penning-discharge SPS at LANL [58].

(RAL) to provide charge-exchange injection into the rapid cycle synchrotron ISIS, a high-power neutron generator [65, 66]. The RAL-SPS design is shown schematically in Fig. 40. The dimensions of the gas discharge chamber and the sector magnet are the same as in the Dudnikov-type source shown

in Fig. 22. A photo of the RAL-PD-SPS is displayed in Fig. 41.

The evolution of the intensity of an H^- ion beam from the RAL SPS PD is shown in Fig. 42a. It took a decade to increase the H^- beam current from 3 mA in 1981 to 40 mA in 1991. Typical oscillograms of discharge voltage, discharge current, H^- ion current, extractor voltage, and total current in the extraction circuit are shown in Fig. 42b. During the first 200 μs, the discharge produces noise; therefore, the H^- beam is extracted during the quieter second half of the discharge. The timeframe of continuous operation is up to 50 days with a pulsed H^- ion current $I^- = 45$ mA and duty cycle of 2.5%. The H^- current was increased later to 70 mA at a pulse duration of up to 1.5 ms and repetition rate of 50 Hz [67].

Based on the RAL SPS, a Penning-discharge SPS was developed for the Chinese spallation neutron source [68]. Examples of oscillograms that characterize operation of the source are shown in Fig. 43. The H^- beam current is 54 mA. The discharge in this SPS is very noisy, so the H^- beam emittance is large.

10.3 Large volume surface plasma sources with self-extraction

A large volume SPS (LV SPS) with a self-extracted H^- beam [69] was developed by Ehlers and Leung at the US-based Lawrence Berkeley National Laboratory (LBNL) in 1981 [69]. A schematic of this source is shown in Fig. 44a. This SPS consists of a large (37.5 liter) gas-discharge chamber with a permanent-magnet multipole magnetic wall, heated cathodes, a cooled molybdenum converter for producing negative ions, a cesium supply system, and an output aperture with magnets to retain electrons. The converter dimensions are 8×25 cm. The back side of the converter and converter holders are shielded with ceramics. The dimensions of the output aperture are 3×25 cm. A photo of this source is displayed in Fig. 44b. Hydrogen is injected into the chamber to a
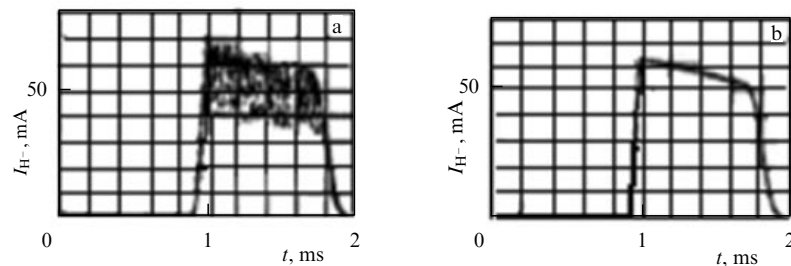

Figure 38. Oscillograms of the H^- beam from a Penning-discharge SPS without nitrogen added (a) and with the addition of 0.46 cm^3 per minute (1%) of nitrogen [61].
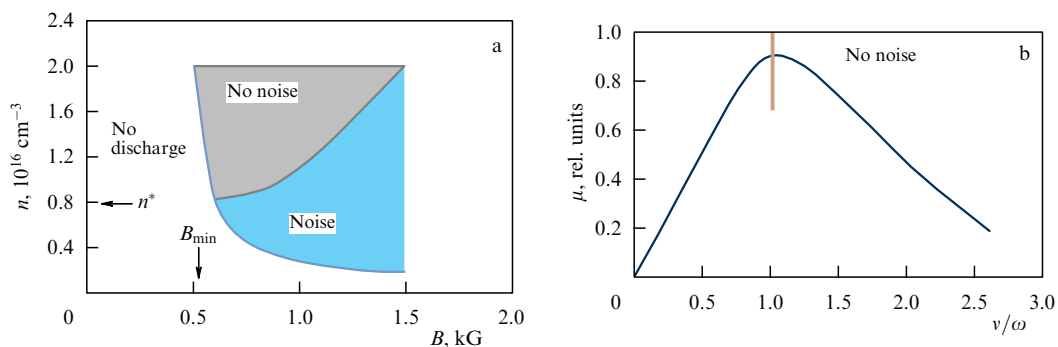

Figure 39. (Color online.) (a) Diagrams of discharge ignition and burning with and without noises in crossed fields in the n, B coordinates. (b) Mobility of electrons as a function of relative scattering frequency [13].
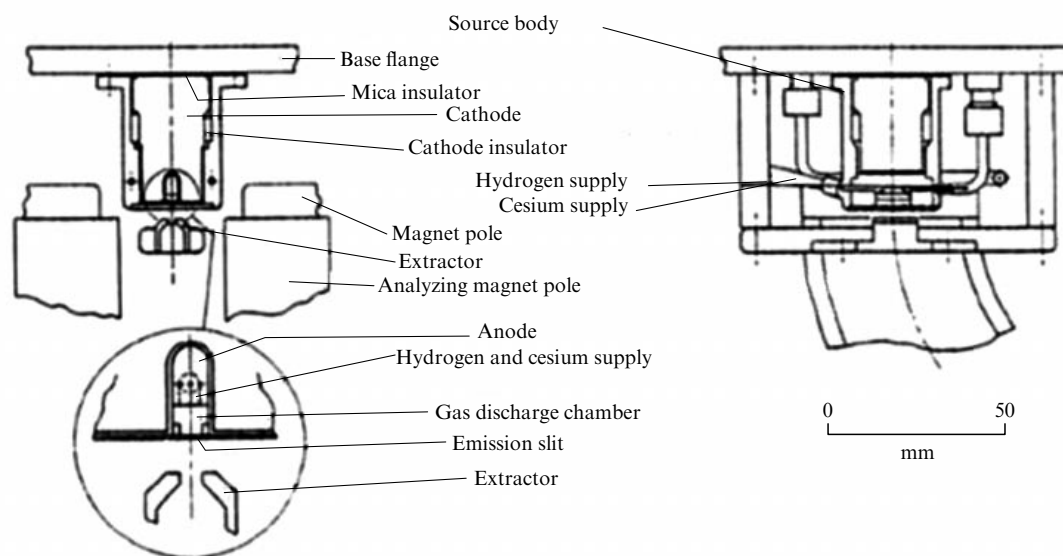
Figure 40. Layout of the RAL-SPS with a Penning discharge [65].
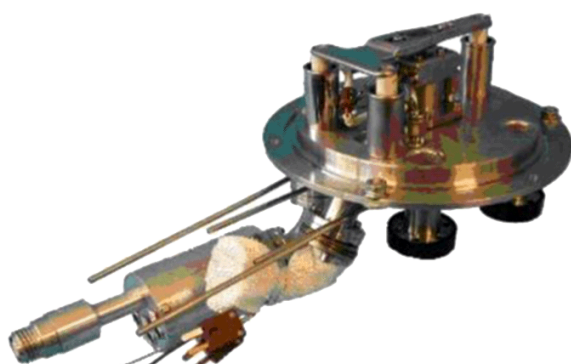

Figure 41. Photo of the RAL-PD-SPS [65].

pressure of 10^{-3} Torr, and a discharge is ignited between the heated cathodes and the wall of the gas discharge chamber using a voltage of ~ 80 V. A potential of -200 V is applied to the converter. Positive ions are accelerated by this potential and bombard the converter, thus causing emission of negative ions. The emitted negative ions are accelerated by this potential difference and directed to the emission aperture, where they are picked up by an extraction voltage of 40 kV. If the discharge current is 145 A, the converter current is 20 A. The negative ion current is 20 mA without cesium, 98% being heavy impurities with high electron affinity. If cesium is added, the negative ion current rapidly reaches 1 A, with an impurity ion level of 1%.

SPS operation with cesium is illustrated in Fig. 45. The estimated gas efficiency of this source is 13%. Based on this
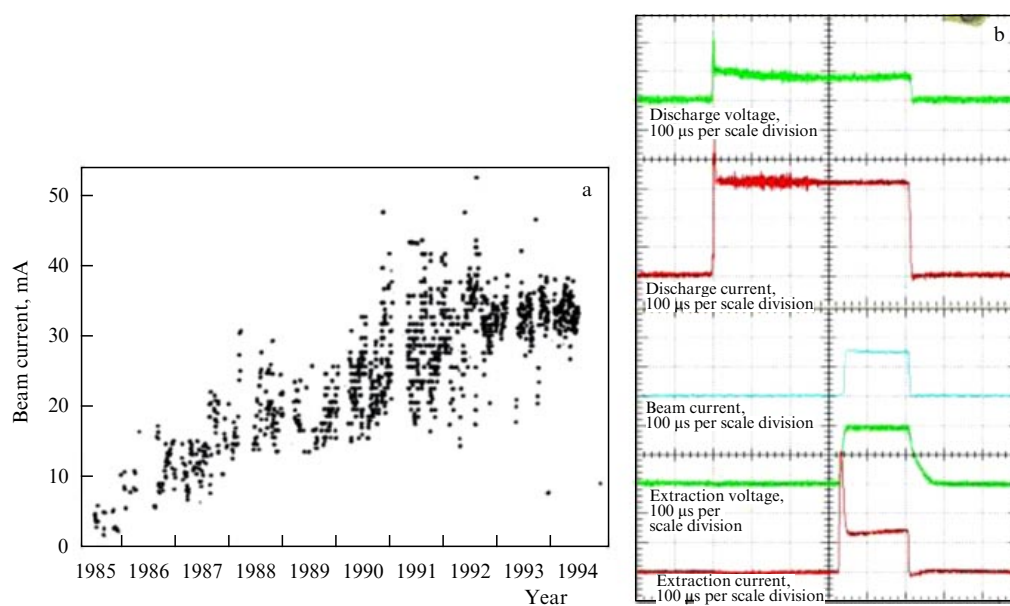

Figure 42. (Color online.) (a) Evolution of the H^- ion beam current from the RAL SPS [66]. (b) Oscillograms of discharge voltage, discharge current, H^- ion current, and extraction voltage and extractor current in an RAL source [66].
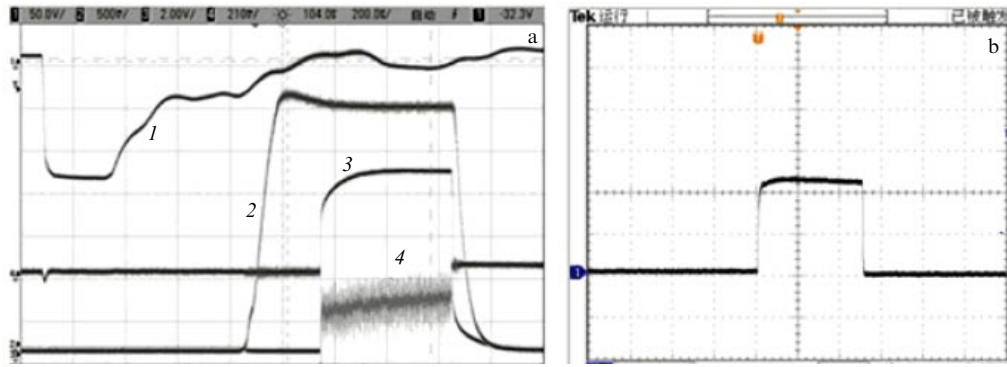
Figure 43. Oscillograms characterizing CSNS-SPS operation [68]: (a) *1* — gate pulse, *2* — discharge current, *3* — extracting voltage pulse of 17 kV, *4* — current in the extracting gap of 240 mA. (b) H⁻ current of 53 mA; horizontal axis — 0.2 ms per scale division.
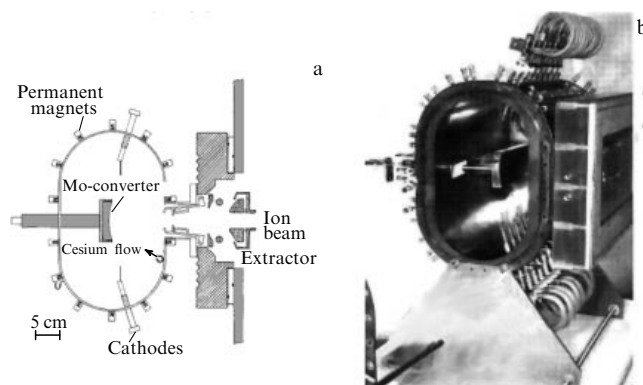

Figure 44. Layout (a) and photo (b) of a large-volume SPS with beam self-extraction [69].
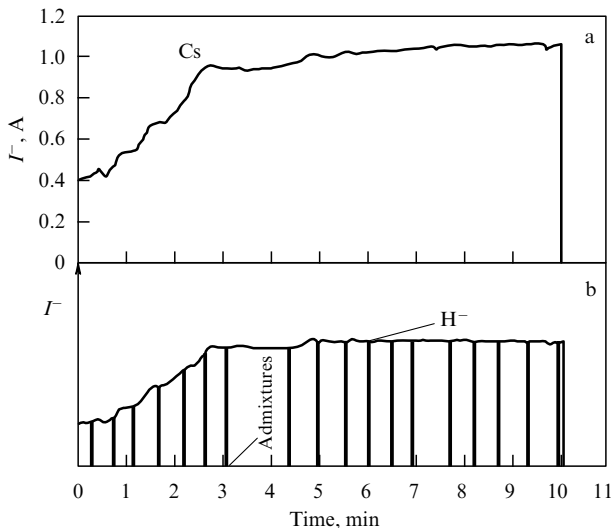

Figure 45. H⁻ ion current in operations of a large-volume SPS with cesium added [69].

Figure 46. Schematic of SPS with a converter operated at the Los Alamos linear accelerator [70]. Dimensions are displayed in inches.

source, an SPS with a converter was developed for the Los Alamos linear accelerator [70]. A schematic of this source is shown in Fig. 46. A large gas-discharge chamber with a multipole magnetic wall is 17.8 cm in diameter and 12.8 cm in height. Two incandescent cathodes 1.5 mm in diameter and 20 cm in length maintain discharge with a voltage of 90, which generates plasma with a density of up to 3×10^{12} cm⁻³. A

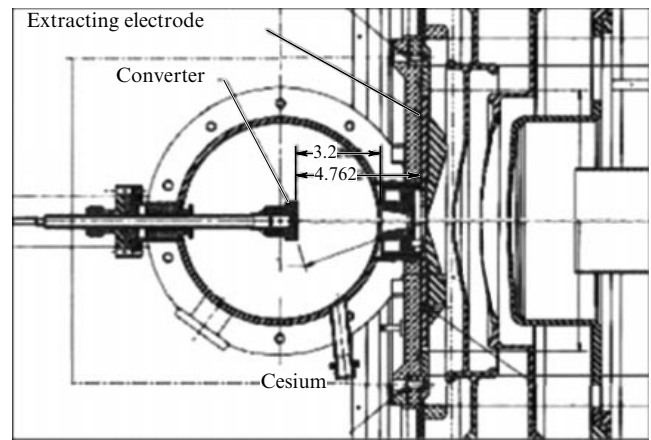cooled converter 5 cm in diameter under a potential of up to −300 V emits negative ions, accelerates them, and focuses them on an emission aperture 6.4 mm in diameter. The distance from the converter emitter surface to the emission aperture is 8.25 cm. Up to 15 mA of H⁻ ions were extracted from this SPS at a duty cycle of up to 10%. The normalized emittance of the beam was $0.13\,\pi$ cm mrad. This source features a high consumption of cesium (up to 1 g per day), whereas other SPSs consume cesium in amounts of less than 1 mg per hour. Along with negative ions, up to 20% of the electron current is also extracted.

A similar source was developed in 1985 for the linear accelerator injector at the KEK facility (Japan Center for Nuclear Research) [71]. This SPS with a converter intended for the KEK linear accelerator consists of a large gas-discharge chamber with a multipole magnetic wall, two direct-heated cathodes made of lanthanum hexaboride, a cooled molybdenum converter 5 cm in diameter and curvature radius of 14 cm, a cesium source, and an emission aperture. The cathode current is 130 A, the converter voltage is −500 V, the discharge current is 29 A, and the discharge voltage is 137 V. The H⁻ ion beam current is 21 mA, and the electron current is 90 mA. The service life of the cathode is more than 1000 hours. Up to 40 mA of H⁻ ions were extracted at a discharge current of 40 A. To ensure stable operation, long-time discharge conditioning is needed for the SPS.

10.4 Surface plasma sources of negative ions with arc discharge for neutral beams under controlled thermonuclear fusion conditions

To create and heat plasma in the Large Helical Device (LHD), a Japan-based stellarator, neutral beams are used on the basis of negative-ion SPSs with cesiation and arc discharges [72].

Following Novosibirsk's example [5], cesium was added in 1990 [73] to the tandem source of negative ions, and a large increase in the emission of negative ions was obtained with a simultaneous significant decrease in the current of accompanying electrons. The H$^-$ ion current as a function of discharge current for discharges with and without cesium is shown in Fig. 47. Subsequent experiments showed that the increase in negative-ion emission is due to activation of the surface plasma mechanism of negative ion formation on the plasma electrode, the work function of which is lowered due to adsorption of cesium. A schematic of the high current SPS for negative ion production is shown in Fig. 48. The H$^-$ ion beam energy is 150 keV, and the beam current is 40 A. The discharge chamber, whose dimensions are 35×145 cm with a
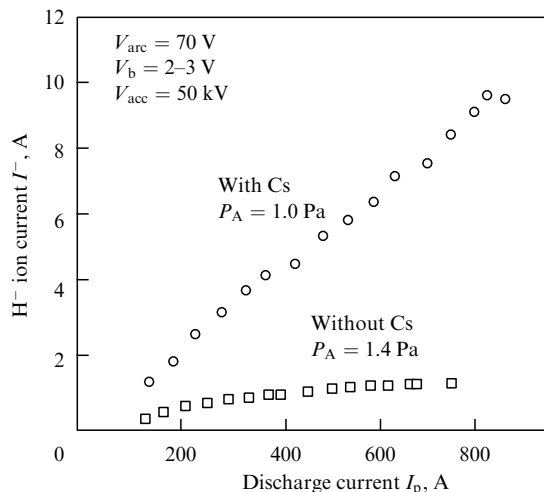

Figure 47. H$^-$ ion current as a function of discharge current for discharges with and without cesium [73]. V_{arc} — discharge voltage, V_b — plasma electrode voltage, V_{acc} — accelerating voltage, and P_A — gas pressure.
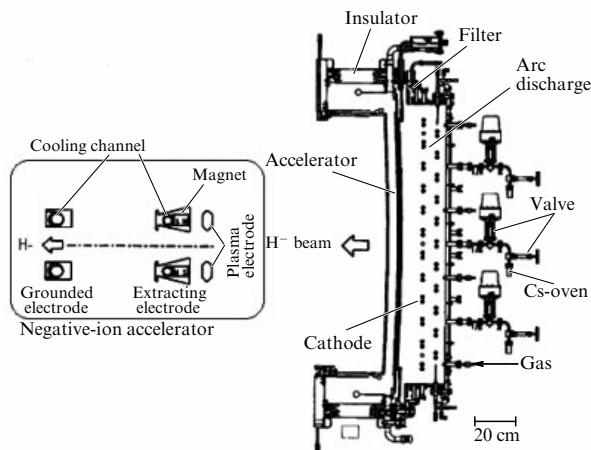

Figure 48. Schematic of a negative-ion SPS with a magnetic wall and arc discharge with cesiation [72].

depth of 21 cm, is equipped with an external magnetic filter. The chamber is surrounded by a multipole magnetic wall, a magnetic filter with a magnetic induction of 50 G. Twenty-five tungsten cathodes maintain a discharge whose power is more than 200 kW, and three cesium ovens control the supply of cesium by varying the temperature.

The accelerating system consists of 3 electrodes: plasma-generating, extracting, and accelerating. The extracting electrode contains embedded permanent magnets to suppress the flux of accompanying electrons (see Fig. 48). Such SPSs have been actively used for injecting high-energy neutral beams since 1998. A general view of the LHD injection system with neutral-beam injectors based on negative-ion SPSs is shown in Fig. 49.

Neutral-beam injectors with an energy of up to 500 keV based on the SPS with cesiation have been designed to heat the plasma and maintain current in the Japan-based JT-60 tokamak [74]. The design and an image of these injectors are displayed in Fig. 50. The setup of SPS-based injectors on the JT-60 tokamak is shown in Fig. 51.

The nominal energy of the beam is 500 keV and the nominal D$^-$ current is 22 A. The magnetic filter is formed by a current of 3–5 kA passing through a plasma grid. The SPS dimensions are: 2 m in diameter and 1.7 m in height. A molybdenum plasma electrode with the dimensions of 45×110 cm is divided into 5 segments with 216 apertures. Three-step acceleration is performed by a six electrode system. A multipole magnetic wall and minimized surface-to-volume ratio enable the discharge to be maintained with incandescent cathodes at a low gas pressure of < 0.3 Pa.

10.5 Development of high-frequency surface plasma sources for the International Thermonuclear Experimental Reactor

An RF SPS with cesiation for the generation of D$^-$ ion beam with an energy of 1 MeV and current of 40 A for the ITER (International Thermonuclear Experimental Reactor) was designed at the Max-Planck Institute for Plasma Physics (MP IPF) [75, 76]. Stages of the development of the RF SPS for the ITER are shown in Fig. 52. The ELISE (Extraction from a Large Ion Source Experiment) SPS is under development at MP IPF in Garching (Germany); it is a half-size ITER SPS intended for continuous-discharge operations that generates 20 A of H$^-$, D$^-$ at a beam extraction voltage of 60 kV for 10 seconds. The SPIDER (Source for Production of Ion of Deuterium Extracted from Rf plasma) SPS currently under development in Padua (Italy) is a full-size ITER SPS with 40 A of H$^-$, D$^-$ with an extraction voltage of 100 kV for 3600 s. MITICA (Megavolt ITER Injector & Concept Advancement) SPS is also being developed in Padua as a full-size ITER RF SPS generating 40 A of H$^-$, D$^-$ ions at 1 MeV for 3600 s. A diagnostic SPS for ITER under development at Gandhinagar (India) will produce H$^-$ ions with an energy of 100 keV and current of 40 A for 3600 s.

A schematic of a high-frequency SPS with an expander and suppression of accompanying electrons is shown in Fig. 53. It consists of a high-frequency plasma generator (1 MHz up to 100 kW) with an Al$_2$O$_3$ ceramic gas-discharge chamber and a Faraday screen, an expansion chamber with a multipole magnetic wall and an external magnetic filter, cesium vaporizers, a plasma electrode, an extraction electrode, and a grounded electrode.

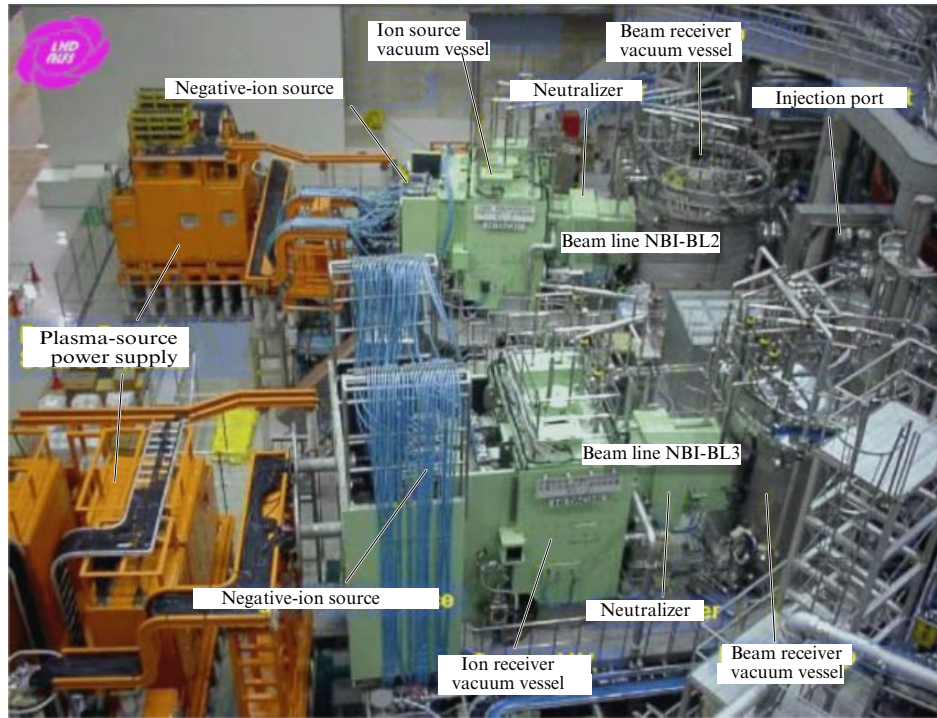The structural scheme of the BATMAN (BAvarian Test MAchine for Negative ions) RF SPS with an expander and

Figure 49. (Color online.) General view of the LHD injection system with SPS-based injectors of neutrals [72].
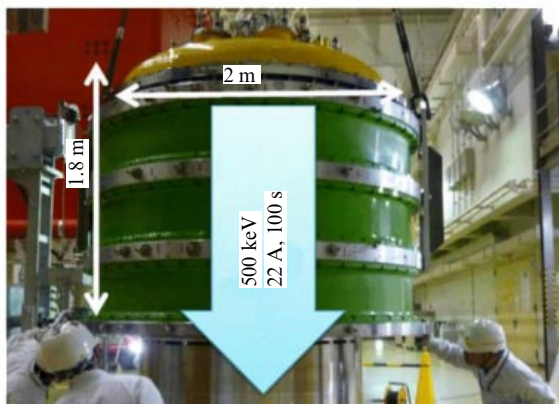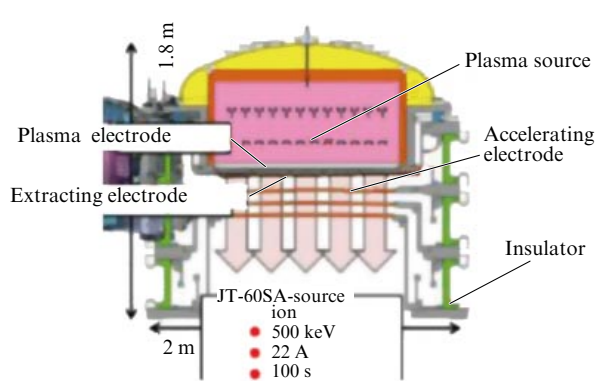

Figure 50. (Color online.) Schematic (a) and photo (b) of injectors based on an SPS with cesiation for JT-60 [74].

Figure 51. (Color online.) Location of SPS-based injectors on the JT-60 tokamak [74].

Figure 52. (Color online.) Stages of RF SPS development for ITER [75].

suppression of accompanying electrons is shown in Fig. 54a. The diameter of the plasma generator is 24 cm, its height is 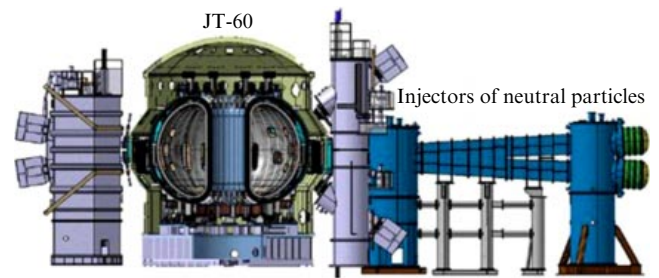15 cm, and the dimensions of the expansion chamber are $32 \times 59 \times 23$ cm. The plasma electrode, whose area is 306 cm^2, has 406 apertures.

The current density of an H$^-$ ion beam as a function of the extraction voltage for various emission areas is shown in Fig. 54b. Permanent magnets are inserted into the extraction electrode to suppress the accompanying electron flow. The extraction voltage is up to 10 kV, and the accelerating voltage is up to 60 kV. The emission current density is up to 32 mA cm^{-2}, and the total H$^-$ current is 9.7 A.

The structure of the ELISE SPS (1/2 ITER SPS) is shown in Fig. 55. It consists of four RF plasma generators, each
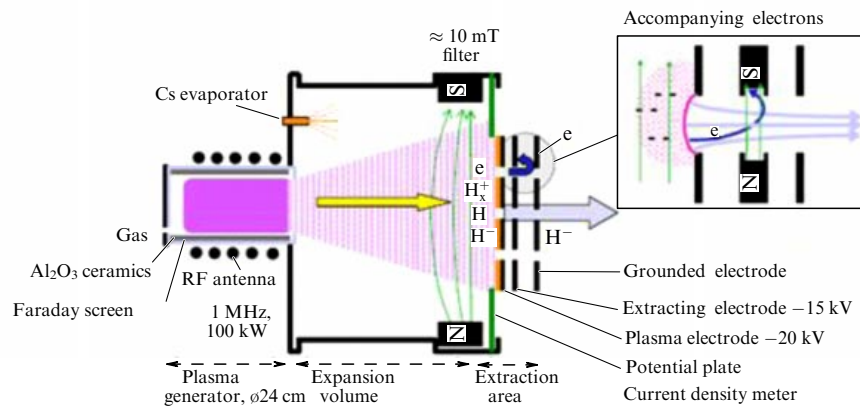
Figure 53. (Color online.) Schematic of an RF SPS with an expander and suppression of accompanying electrons [76].
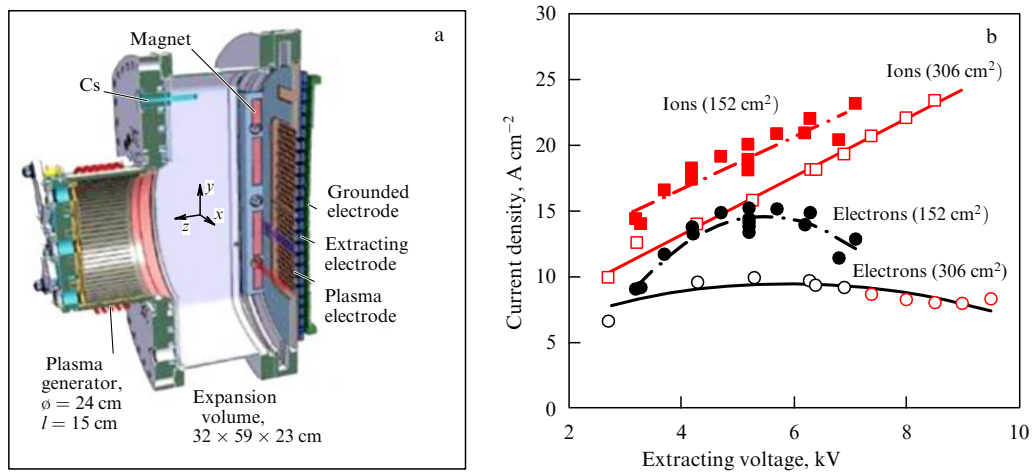

Figure 54. (Color online.) (a) Structural design of BATMAN RF SPS with an expander and suppression of accompanying electrons (1/8 ITER SPS) [75]. (b) Current density of H^- I ions and accompanying electrons as a function of extracting voltage for various emissions areas [76].

Figure 55. Structural design of SPS ELISE (1/2 ITER SPS) [76].

28.4 cm in diameter, a holder for the extraction system, an expansion chamber with diagnostic ports, a plasma electrode, an extraction electrode, and a grounded electrode. The chamber is pumped out by two cryogenic pumps at a pumping rate of $2 \times 350,000 \ \mathrm{l \ s^{-1}}$. A magnetic filter is created by the current flowing through the plasma electrode.

Figure 56. Structural design of the RF SPS for ITER [77].

Figure 57. Structural design of neutral beam injector based on an RF SPS with cesiation for ITER [78]: (a) isometric view of the injector, (b) section of the injector.
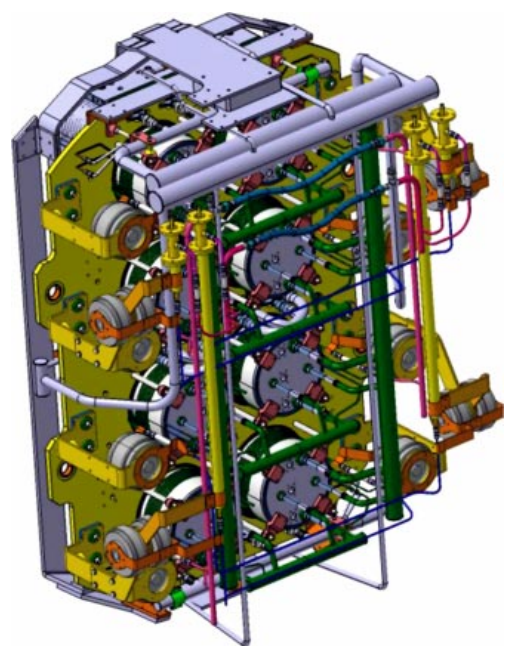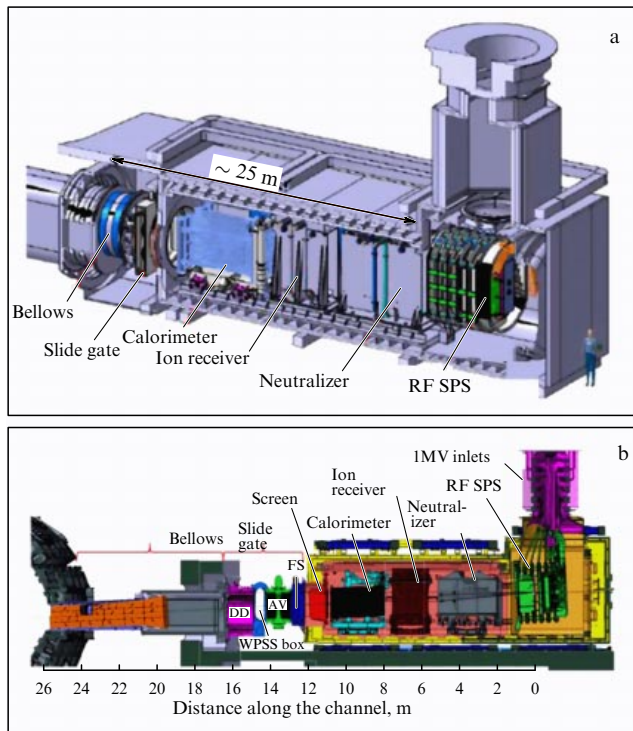
The RF plasma generators are 2×180 kW, and the H$^-$ ion current is 20 A. A Faraday screen, plasma electrode, and potential electrode are coated with 3 μm of molybdenum.

A schematic of the structure of the RF SPS for ITER is shown in Fig. 56. It contains eight plasma generators, a plasma electrode, and a five-stage acceleration system. The structural design of the neutral-particle injector with an RF SPS for ITER is shown in Fig. 57. It consists of an RF SPS for the generation of 70 A of negative H$^-$ ions or 39 A of D$^-$ ions, a system accelerating up to 1 MeV, a gas neutralizer, residual-ion receivers, a calorimeter for measuring beam intensity, and a gate valve and bellows.

The estimated cost of three injectors with an RF SPS is ~ 1 billion US dollars.

11. General comments on the surface plasma method for the production of negative-ion beams

One of the practical results brought by the development of high-brightness SPSs is the wide use of charge-exchange injection in accelerators. SPSs are now 'sources of life' and 'workhorses' for major accelerator facilities: SNS (Spallation Neutron Source) at Oak Ridge National Laboratory (ORNL), Fermi National Accelerator Laboratory (FNAL), Brookhaven National Laboratory (BNL), Los Alamos Neutron Scientific Center (LANSCE), Rutherford–Appleton Laboratory (RAL), Large Hadron Collider (LHS) at CERN, Japanese proton complex (KEK-J-PARC), and Deutsches Elektronen-Synchrotron (DESY). Charge exchange injection is used at the CELSIUS storage ring (Uppsala, Sweden) [77] and COSY storage ring (Research Center based in Jülich, Germany) [78, 79]. Charge exchange injection was used in the synchrotron operated at the

A I Alikhanov Institute of Theoretical and Experimental Physics for the accumulation of carbon ions [80]. A transition to charge-exchange injection is now under preparation at the CERN booster (Switzerland) [81], the IHEP booster (Protvino, Russia) [82], and other accelerators. Developments in charge-exchange injection are reviewed in [83, 84].

The efficiency and operational reliability of these SPSs determine the efficiency of the listed research laboratories. Many discoveries in high-energy physics have been made using SPSs.

The development of high-brightness SPSs was first stimulated by the successful accumulation of intense proton beams using charge-exchange injection [12]. It was supported later by the interest in particle beam weapons in space as an element of 'Star Wars' [85]. Testing of the acceleration and neutralization of H$^-$ ions in space is described in the Beam Experiment Aboard Rocket (BEAR) report [86, 87]. Due to the military nature of applications and information being classified, the first publications were significantly delayed; however, informal contacts were relatively fast. Attention was focused until 1971 on charge-exchange sources, since there was no hope of extracting more than 5 mA of H$^-$ ions from plasma.

The cesiation effect, a significant enhancement of negative ion emission with a concurrent decrease in accompanying electron current to a level less than the negative ion current, was observed for the first time on July 1, 1971 at the Novosibirsk-based G I Budker Institute of Nuclear Physics, when a compound containing 1 mg of cesium was introduced into the discharge in a planotron [4]. This effect was further developed to become a basis of a conceptually new surface plasma method of negative-ion production [4, 13]. The patent application states: "a method of negative ion production in gas discharges, comprising addition to the discharge, apart from a working medium, of an admixture of a substance with a low ionization potential such as, for example, cesium for enhancement of negative ion formation" [4].

Subsequent experiments showed that adsorption of cesium decreases the surface work function from 4–5 eV to 2–1.6 eV, thus enhancing secondary emission of negative ions caused by bombarding the surface by plasma particles, i.e., surface-plasma generation of negative ions. Ion sources based on this process were named 'surface plasma sources of negative ions (SPSs)'. A theoretical explanation of this enhancement has been suggested by Kishinevskii [88]. In the problem of interest for us, the shift of electron affinity levels when a particle approaches a surface, which is due to interaction between the electron and a metal, has a dominant effect on the resulting interaction between the particle and the surface. In the studies cited above, the shift of the electron affinity with respect to the Fermi level was approximated by the effect of the image potential force. In approaching the surface, the electron affinity level is transformed into an acceptor level band, and the center of this band descends with respect to the level of electron affinity of free particle S by a value of $\Delta S = e^2/4x$, while the valence electron level for particles with small ionization energy V is transformed into a donor level band whose center elevates with respect to V by $\Delta V = e^2/4x$. Thus, electron affinity as a function of the distance between the particle and the surface x is approximated by the formula

$$S(x) = S + \frac{e^2}{4x} \, .$$

If the difference between the work function φ and electron affinity S is not too large, at distances accessible for the particles $x < x_0 = e^2/4(\varphi - S)$, the electron affinity levels fall below the Fermi level for a solid state. As a result, the probability of resonance population of this level by solid-state electrons becomes close to one, in accordance with the thermodynamically equilibrium Fermi distribution. If particles move away from the $x < x_0$ region, some of them may escape in the form of negative ions. In the $x > x_0$ region, an energy that is larger than that for a neutral particle by a value of $\Delta l = \varphi - S$ is needed to remove an ion from the surface. Owing to this, the electron level in a free negative ion proves to be higher than the Fermi level in the solid state by $\varphi - S$. The electron is delivered to the electron affinity level due to the kinetic energy of the particle moving away. A similar situation occurs in charge exchange in atomic collisions when a bound electron is recaptured to a level with a smaller binding energy.

A small admixture of cesium or another substance with a low ionization potential to the gas discharge significantly increases the emission of negative ions [89]. If done correctly, cesiation works perfectly well. However, improper cesiation can complicate ion source operation. For example, the injection of excessive cesium may cause a breakdown in the extractor.

Further development of the SPS was conducted by the Belchenko, Dimov, and Dudnikov team. The development of a high-brightness SPS has been described by the author in [13, 34]. The semiplanotron SPS with effective geometric focusing has been developed by the author [90]. Development and adaptation of SPSs commenced at many laboratories based in the US, Europe, and Japan. Brookhaven (BNL) symposia and European conferences on the production and use of light negative ions were established, to be replaced later by the International Symposium on Negative Ions and Beams (NIBS).

The physical principles of SPS operation were published in [5] and after that reproduced in many reviews and books. A good overview of SPSs for accelerators was presented in Peters's reports [46]. Early work on SPSs was reviewed by N Wells [91]. The work of the Allison group in Los Alamos is reported in [92]. The development of high-current SPSs for thermonuclear research was conducted at LBNL and in Japan, where this work is in progress, and the sources are used to inject neutrals into the JT-60 tokamak and the LHD stellarator. The author proposed to produce polarized negative ions by resonant charge exchange on slow negative deuterium ions obtained by the surface plasma method; this has been implemented in cooperation with Belov [93].

The development of SPSs for the production of heavy negative ions was successful; however, stationary SPSs for industrial applications still require some improvements. An SPS for long-term operation was developed at the Institute of Nuclear Physics of the Siberian Branch of the Russian Academy of Sciences. Cesiated SPSs for accelerators have been significantly improved by the SNS ion source group at ORNL. RF SPSs for controlled thermonuclear fusion have been significantly advanced by the MP INF group. The historical development of negative-ion sources and the growth of beam current with time is shown in Fig. 58.

Many SPS versions have been developed and optimized for a variety of applications. The addition of cesium enhances the formation of negative ions in all types of discharge. However, the production of high-brightness negative-ion
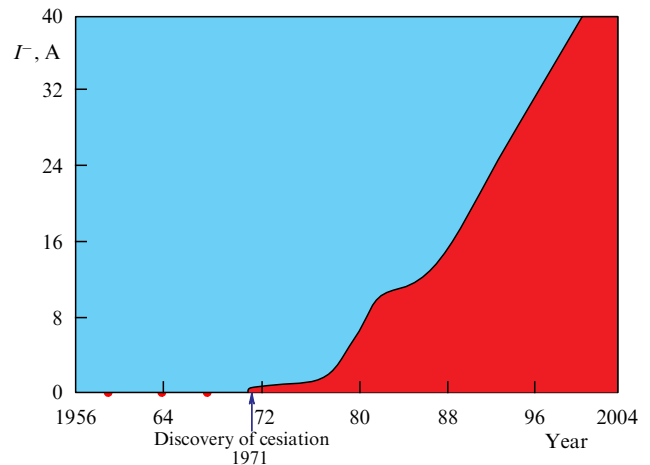

Figure 58. History of the development of negative-ion sources. Growth of beam intensity with time.
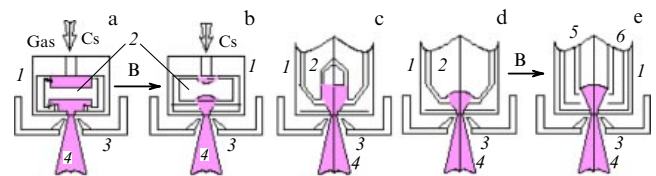

Figure 59. (Color online.) Layouts of basic versions of compact SPSs: (a) planar magnetron-planotron, (b) magnetron with geometric focusing, (c) Penning discharge SPS — Dudnikov source, (d) semiplanotron, (e) SPS with a hollow cathode.

Figure 60. (Color online.) Schematics of the main versions of discharges in large volume SPSs: (a) SPS with a multipole magnetic wall and a converter; (b) SPS with the formation of negative ions on the plasma electrode; (c) RF SPS with anodic generation of negative ions; (d) RF SPS with an emitter; (e) RF SPS with an external antenna; (f) SPS for production of polarized negative ions.

beams proves to be most efficient in dedicated SPSs optimized for various applications. Some base configurations of discharges in compact SPSs are shown in Fig. 59.

The main components of the SPS displayed in Figs 59 and 60 are *1* — anode (gas-discharge chamber); *2* — cold cathode (emitter); *3* — extractor with a magnet system; *4* — ion beam; *5* — independent emitter; *6* — hollow cathode; *7* — heated

Table. Modern high-current sources of H$^-$ ions for accelerators.

Source*	SPS type	Discharge parameters	Frequency, Hz	Duty factor, %	Pulsed current, mA	Aperture, mm	Service life, h	Service life, A h
BNL	Magnetron	12 A 130 V	7.5	0.5	120	2.8 $\varnothing$	5760	3.0
FNAL	Magnetron	15 A 180 V	15	0.35	80	3.2 $\varnothing$	6500	3.2
RAL	Penning	55 A 70 V	50	3.75	55	0.6 × 10	840	0.51
CSNS	Penning	50 A 100 V	25	1.5	50	0.6 × 10	720	0.46
INP RUS	Penning	100 A 120 V	50	1.25	50	1 × 10	600	0.45
LANSCE	Converter	35 A 180 V	120	10	18	6.8 $\varnothing$	670	0.87
SNS	RF internal	60 kW 2 MHz	60	6.0	60	7 $\varnothing$	4400	7
J-PARC	RF internal	30 kW 2 MHz	25	2.5	90	9 $\varnothing$	1850	2.0
CERN	RF external	40 kW 2 MHz	0.8	0.07	45	5.5 $\varnothing$	1200	0.026

*BNL — Brookhaven National Laboratory, USA; FNAL — Fermi National Accelerator Laboratory, USA; RAL — Rutherford Appleton Laboratory, UK; CSNS — China Spallation Neutron Source, China; INR RAS — Institute of Nuclear Research of the Russian Academy of Sciences; LANSCE — Los Alamos Neutron Science CEnter, USA; SNS — Spallation Neutron Source, USA; J-PARC — Japan Proton Accelerator Research Complex, Japan; CERN — European Organization for Nuclear Research, Switzerland.

cathode; 8 — multipole magnetic wall; 9 — RF antenna; and 10 — magnetic filter.

The compact SPSs displayed in Fig. 59 use glow discharges with cold cathodes in crossed $E \times B$ fields. These SPSs feature high plasma density (up to 10^{14} cm^{-3}), high emission density of negative-ion current (up to 8 A cm^{-2}), and small gaps (1–5 mm) between the emitter cathode and the emission aperture in the anode. They are simple, exhibit high energy efficiency (up to 100 mA kW^{-1}), and have high gas efficiency (up to 30%) with a pulsed gas valve. Compact SPSs perfectly fit for operations in a pulsed mode, although they have also been successfully used for stationary-mode operations with a current emission density of up to 300 mA cm^{-2} and up to 1 A cm^{-2}.

The situation with large volume SPSs whose discharge volume is tens and up to hundreds of liters is different. Schematic of the main versions of discharges in large-volume SPSs are displayed in Fig. 60. SPSs where negative ions are produced on the plasma electrode (Fig. 60b) are used to generate H$^-$ for controlled thermonuclear fusion with a current of up to 70 A. RF SPSs with anode generation (Fig. 60c) are used in SPSs for accelerators. RF SPSs with an emitter (Fig. 60d) are intended for the generation of heavy negative ions. RF SPSs with an external antenna (Fig. 60e) are used in SPSs for accelerators and controlled thermonuclear fusion.

The Table displays characteristics of modern high-current sources of H$^-$ ions for accelerators. The most intense H$^-$ ion beam is obtained from the BNL magnetron SPS (up to 100–120 mA) with a service life of up to 3 A h. The longest service life is exhibited by the RF SPS of the Spallation Neutron Source (SNS) at Oak Ridge: up to 7 A h (20 weeks with an H$^-$ beam current of 60 mA at a duty cycle of 6%) [94].

A description of how injectors of neutrals for the ITER have been developed may be found in [95]. The development of injectors of ions and neutrals and the surface-plasma method for producing negative-ion beams at the G I Budker Institute of Nuclear Physics of the Siberian Branch of the Russian Academy of Sciences is reviewed in [96, 97]. The most recent reviews of negative-ion sources are published in [98, 99]. The most recent accomplishments in the development of negative-ion sources are reviewed in [100].

12. Conclusion

Since the discovery of the surface plasma mechanism of negative ion formation with cesiation, many modifications of the SPS have been developed, and many improvements have been introduced, so that now surface plasma method is a proven technology. Many teams of highly skilled researchers, engineers, workers, and administrators all over the world are engaged in the development and use of SPSs with cesiation. The intensity of negative-ion beams has increased by a factor of 10^4, from a record-setting 3 mA to more than 40 A. The cost of advanced injectors has soared from thousands to millions USD. Major projects are now ongoing where SPSs for the Large Hadron Collider and ITER are being developed. The development and manufacture of SPSs with cesiation is now a business whose turnover is of the order of a billion USD [101].

References

1. Gabovich M D *Fizika i Tekhnika Plazmennykh Istochnikov Ionov* (Physics and Technology of Plasma Ion Sources) (Moscow: Atomizdat, 1972)
2. Dudnikov V, Westner A *Rev. Sci. Instrum.* **73** 729 (2002)

3. Dimov G I, Dudnikov V G *Sov. J. Plasma Phys.* **4** 3 (1978); *Fiz. Plazmy* **4** 3 (1978)

4. Dudnikov V G "Sposob polucheniya otritsatel'nykh ionov" ("A method for production of negative ions"), USSR Patent, M. Cl.H 01 J 3/0,4, 411542, application 10/III,1972; https://inis.iaea.org/search/search.aspx?orig_q = RN:9355182

5. Belchenko Yu, Dimov G, Dudnikov V "Physical principles of surface plasma source operation", in *Symp. on the Production and Neutralization of Negative Hydrogen Ions and Beams, Brookhaven, 1977* (New York: Brookhaven Natl. Laboratory, 1977) p. 79

6. Nagashima Y M K et al. "Positronium negative ion experiments — formation, photodetachment and production of an energy tunable positronium beam", in *XXVII Intern. Conf. on Photonic, Electronic and Atomic Collisions, ICPEAC 2011*; *J. Phys. Conf. Ser.* **388** 012021 (2012)

7. Dudnikov V, Dudnikov A *AIP Conf. Proc.* **1869** 020007 (2017)

8. Dudnikov V, Dudnikov A *AIP Conf. Proc.* **2052** 060001 (2018)

9. Woodcock K *Phys. Rev.* **38** 1696 (1931)

10. Arifov U A, Ayukhanov A Kh *Izv. Akad. Nauk Uz. SSR, Ser. Fiz.-Mat. Nauk* **6** 34 (1961)

11. Kron V E *J. Appl. Phys.* **34** 3523 (1962)

12. Budker G, Dimov G, Dudnikov V *Sov. Atom. Energy* **22** 441 (1967); *Atom. Energ.* **22** 348 (1967); in *Proc. Intern. Symp. on Electron and Positron Storage Ring, France, Saclay, 1966*, Rep. VIII, 6.1; Dudnikov V G "Poluchenie intensivnogo protonnogo puchka v nakopitele metodom perezaryadnoi inzhektsii" ("Production of intense proton beam in storage ring by charge exchange injection method"), Thesis for the Degree of Cand. Sci. (Phys.-Math.) (Novosibirsk: Institute of Nuclear Physics of the Siberian Branch of the USSR Academy of Sciences, 1966); Dudnikov D, arXiv:1808.06002

13. Dudnikov V G "Poverkhnostno-plazmennyi metod polucheniya puchkov otritsatel'nykh ionov" ("Surface-plasma method for production of negative-ion beams"), Thesis for the Degree of Dr. Sci. (Phys.-Math.) (Novosibirsk: Institute of Nuclear Physics of the Siberian Branch of the USSR Academy of Sciences, 1977)

14. Derevyankin G E, Dudnikov V G, Zhuravlev P A *Prib. Tekh. Eksp.* (5) 168 (1975)

15. Belchenko Yu I "Emissiya otritsatel'nykh ionov iz sil'notochnykh razryadov" ("Emission of negative ions from high-current discharges"), Thesis for the Degree of Cand. Sci. (Phys.-Math.) (Novosibirsk: Institute of Nuclear Physics of the Siberian Branch of the USSR Academy of Sciences, 1974)

16. Belchenko Yu I et al. *Dokl. Akad. Nauk SSSR* **213** 1283 (1973)

17. Belchenko Yu I, Dimov G I, Dudnikov V G *Izv. Akad. Nauk SSSR. Ser. Fiz.* **37** 2573 (1973); Belchenko Yu, Dimov G, Dudnikov V *Nucl. Fusion* **14** 113 (1974)

18. Dimov G I, Roslyakov G V, Savkin V Ya *Prib. Tekh. Eksp.* (4) 29 (1977)

19. Komarov V L et al., in *Dokl. Vsesoyuz. Soveshchaniya po Inzhenernym Problemam* (Proc. All-Union Workshop on Engineering Problems) Vol. 1 (Leningrad: UTS, NIIEFA, 1975)

20. Komarov V L, Strokach A P, Preprint D-0282 (Leningrad: NIIEFA, 1976)

21. Belchenko Yu I, Dudnikov V G, Preprint 77-56 (Novosibirsk: Institute of Nuclear Physics of the Siberian Branch of the USSR Academy of Sciences, 1977)

22. Belchenko Yu I, Dudnikov V G, in *4-ya Vsesoyuz. Konf. po Vzaimodeistviyu Atomnykh Chastits s Tverdym Telom* (Proc. 4th All-Union Conf. on Interaction of Atomic Particles with Solid State) Vol. 3 (Kharkov, 1967) p. 180

23. Dudnikov V G, Obrazovskii E G, Fiksel' G I, Preprint 77-50 (Novosibirsk: Institute of Nuclear Physics of the Siberian Branch of the USSR Academy of Sciences, 1977); *Sov. J. Plasma Phys.* **4** 370 (1978); *Fiz. Plazmy* **4** 662 (1978)

24. Stakhanov N P (Ed.) *Fizicheskie Osnovy Termoemissionnogo Preobrazovaniya Energii* (Physical Basis of Thermoemission Converters) (Moscow: Atomizdat, 1973)

25. Moizhes B Ya, Pikus G E (Eds) *Termoemissionnye Preobrazovateli i Nizkotemperaturnaya Plazma* (Thermoemission Converters and Low Temperature Plasma) (Moscow: Nauka, 1973)

26. Papageorgopolous C A, Chen J *J. Phys. C* **6** L279 (1973)

27. Pivovarova G Ya, Saminskii L A *Tekhnologicheskie Protsessy Elektrovakuumnogo Proizvodstva* (Electrovacuum Production Processes and Technology) (Moscow: Energiya, 1975) p. 192

28. Belchenko Yu et al. *Zh. Tekh. Fiz.* **3** 282 (1977)

29. Dimov G I, Derevyankin G E, Dudnikov V G *IEEE Trans. Nucl. Sci.* **24** 1545 (1977)

30. Dudnikov V, Chapovsky P, Dudnikov A *Rev. Sci. Instrum.* **81** 02A714 (2010)

31. Aliev A A et al. *Tech. Phys.* **55** 111 (2010); *Zh. Tekh. Fiz.* **80** (1) 110 (2010)

32. Murin B P, in *Proc. of the 7th Intern. Conf. on High Energy Accelerators, CERN* (1971) p. 540

33. Avramenko M I et al., in *Trudy Vsesoyuz. Soveshchaniya po Uskoritelyam Zaryazhennykh Chastits* (Proc. All-Union Workshop on Accelerators of Charged Particles) Vol. 1 (Moscow: Nauka, 1973) p. 261

34. Dudnikov V G "Istochniki otritsatel'nykh ionov vodoroda s Penningovskoi geometriei" ("Surface plasma source of Penning geometry"), in *Trudy IV Vsesoyuz. Soveshchaniya po Uskoritelyam Zaryazhennykh Chastits* (Proc. 4th All-Union Workshop on Particle Accelerators) Vol. 1 (Moscow: Nauka, 1975) p. 323

35. Prelec K, Sluyters Th, in *Proc. of the 2nd Symp. on Ion Sources and Formation of Ion Beams, Berkeley, Ca.* (1974); LBL-3399

36. Prelec K, Sluyters Th *IEEE Trans. Nucl. Sci.* **22** 1662 (1975)

37. Prelec K, Sluyters Th, Grossman M *IEEE Trans. Nucl. Sci.* **24** 1521 (1977)

38. Alessi J G, Sluyters Th *Rev. Sci. Instrum.* **51** 1630 (1980)

39. Alessi J et al. *IEEE Trans. Nucl. Sci.* **28** 2652 (1981)

40. Schmidt C, Curtis C "Negative hydrogen-ion program at fermilab", in *Proc. of the 1976 Proton Linear Accelerator Conf., Chalk River, Ontario, Canada, 1976* (1976)

41. Schmidt Charles W, Curtis Cyril D *IEEE Trans. Nucl. Sci.* **26** 4120 (1979)

42. Schmidt C W, Curtis C D, in *Proc. of the Symp. on the Production and Neutralization of Negative Hydrogen Ions and Beams, BNL, September 26–30, 1977* (1977) p. 123, BNL50727

43. Curtis C D, Owen C W, Schmidt C W "Factors affecting H-beam performance in the Fermilab Linac", in *41st Proc. of the 1986 International Linac Conf., Stanford, Calif., USA, 1986* (1986)

44. Stipp V, Dewitt A, Madsen J *IEEE Trans. Nucl. Sci.* **30** 2743 (1983)

45. Barton D S, Witkover R L *IEEE Trans. Nucl. Sci.* **28** 2681 (1981)

46. Peters J *Rev. Sci. Instrum.* **69** 992 (1998)

47. Alessi J M et al. "H⁻ source and beam transport experiments for a new RFQ", in *Particle Accelerator Conf., Washington, DC, USA, 1987* (1987)

48. Bollinger D S, Sosa A *AIP Conf. Proc.* **1869** 030054 (2017)

49. Allison Paul W et al. "Status of the Lampf H⁻ Injector", in *Proc. of the 1972 Proton Linear Accelerator Conf., Los Alamos, NM, USA* (1972)

50. Robinson C *Aviation Week Space Tech.* 42 (1978)

51. Bloembergen N et al. "Report to the American Physical Society of the study group on science and technology of directed energy weapons" *Rev. Mod. Phys.* **59** (3) S1 (1987)

52. "Report to the American Physical Society of the study group on science and technology of directed energy weapons. Executive Summary and Major Conclusions" *Phys. Today* **40** (5) S3 (1987)

53. Allison P W "Experiments with Dudnikov type H⁻ source", Preprint LA-UK-77-2113 (Los Alamos, 1977)

54. Allison P W, "Experiments with a Dudnikov type H⁻ ion source", in *Proc. of the Symp. on the Production and Neutralization of Negative Hydrogen Ions and Beams, Upton, New York, September 26–30, 1977*; Report BNL-50727 (Upton, NY: Brookhaven National Laboratory, 1977) p. 119

55. Smith H V (Jr.), Allison P "H⁻ beam emittance measurements for the penning and the asymmetric, grooved magnetron surface-plasma sources", in *Proc. of the 1981 Linear Accelerator Conf., Santa Fe, NM, USA, 1981* (1981)

56. Alisson P, Sherman J "Operation experience with 100 keV, 100 mA injector" *AIP Conf. Proc.* **111** 511 (1981)

57. Smith H V (Jr.) et al. *Rev. Sci. Instrum.* **63** 2723 (1992)

58. Smith H V (Jr.), Allison P, Sherman J D *Rev. Sci. Instrum.* **65** 123 (1994)

59. Smith H V (Jr.), Allison P, Sherman J D *IEEE Trans. Nucl. Sci.* **32** 1797 (1985)
60. Sherman J D, Allison P, Smith H V (Jr.) *EEE Trans. Nucl. Sci.* **32** 1973 (1985)
61. Smith H V (Jr.) "Emission spectroscopy of the 4X source discharge with and without N2 gas", AT-10 Technical Note 89-07 (1989)
62. Sherman J D et al. "Review of scaled penning H⁻ surface plasma source with slit emitters for high duty factor linacs, CP642", in *High Intensity and High Brightness Hadron Beams: 20th ICFA Advanced Beam Dynamics Workshop on High Intensity and High Brightness Hadron Beams* (Eds W Chou et al.) (College Park, MD: American Institute of Physics, 2002)
63. Dudnikov V et al. *AIP Conf. Proc.* **1515** 369 (2013)
64. Leung K N et al. *AIP Conf. Proc.* **158** 356 (1987)
65. Gear P E, Sidlow R, in *Proc. of the 2nd Int. Conf. Low Energy Ion Beams* (Inst. Phys. Con. Ser., No 54) (London: IOP, 1980) p. 284
66. Sidlow R et al. "Operational experience of Penning H⁻ ion sources at ISIS", in *Proc. 5th European Particle Accelerator Conf., EPAC'96, Sitges, Spain, Jun. 1996* (1996) paper THP084L
67. Faircloth D C et al. *Rev. Sci. Instrum.* **79** 02B717 (2008)
68. Liu S-J et al. *Chinese Phys. C* **39** 057008 (2015)
69. Leung K N, Ehlers K W *Rev. Sci. Instrum.* **53** 803 (1982)
70. York R L, Stevens R R *IEEE Trans. Nucl. Sci.* **30** 2705 (1983)
71. Takagi A et al. *IEEE Trans. Nucl. Sci.* **32** 1782 (1985)
72. Koneko O et al., in *Proc. of the 16th Intern. Conf. on Fusion Energy, Montreal* Vol. 3 (1996) p. 539
73. Okumura Y et al., in *Proc. of the 16th Symp. on Fusion Technology, London* Vol. 2 (1990) p. 1026
74. Hanada M et al. *AIP Conf. Proc.* **1396** 536 (2011)
75. Kraus W et al. *Rev. Sci. Instrum.* **75** 1832 (2004)
76. Fantz U et al. *Plasma Phys. Control. Fusion* **49** B563 (2007)
77. Hermanson L et al., in *Proc. of Workshop on Beam Cooling and Related Topics, Montreux, 4–8 October, 1993* (CERN 94-03) (Geneva: CERN, 1994) p. 235
78. Baldin A M, Kovalenko A D *JINR Rapid Commun.* **377** 96 (1996)
79. Sidorin A O "Formirovanie intensivnykh ionnykh puchkov v nakopitelyakh s mnogooborotnoi perezaryadnoi inzhektsiei i elektronnym okhlazhdeniem" ("Formation of intense ion beams in storage rings with multiturn charge-exchange injection and electron cooling"), Thesis for the Degree of Cand. Sci. (Phys.-Math.) (Dubna: JINR, 2003)
80. Alekseev N N, Koshkarev D G, Sharkov B Yu *JETP Lett.* **77** 123 (2003); *Pis'ma Zh. Eksp. Teor. Fiz.* **77** 149 (2003)
81. Lettry J et al. *AIP Conf. Proc.* **1655** 030005 (2015)
82. Frolov B A, Klenov V S, Mihailov V N, in *Proc. of the XXIV Russian Particle Accelerator Conf., RuPAC'2014, Obninsk, Russia, 6–10 October, 2014* (2014) p. 429
83. Dimov G I *Rev. Sci. Instrum.* **67** 3393 (1996)
84. Dudnikov V G *Phys. Usp.* **62** 405 (2019); *Usp. Fiz. Nauk* **189** 433 (2019)
85. Gsponer A "Physics of high-intensity high-energy particle beam propagation in open air and outer-space plasma", physics/0409157
86. Schrage D et al. "Flight-qualified Rfq for the bear project", in *Proc. 1988 Linear Accelerator Conf., Williamsburg, Virginia, USA, 1988* (1988)
87. O'Shea P G et al. "The bear accelerator", in *Proc. of the 1989 IEEE Particle Accelerator Conf., 1989* (1989)
88. Kishinevskii M E *Zh. Tekh. Fiz.* **48** 73 (1978); Preprint INF 76-18 (Novosibirsk: Institute of Nuclear Physics of the Siberian Branch of the USSR Academy of Sciences, 1976)
89. Dudnikov V *Rev. Sci. Instrum.* **83** 02A708 (2012)
90. Dudnikov V, Belchenko Yu, Preprint No. 78-95 (Novosibirsk: Institute of Nuclear Physics of the Siberian Branch of the USSR Academy of Sciences, 1978); *J. Phys. Colloq.* **40** 477 (1979)
91. Wells N "The development of high-intensity negative ion sources and beams in the USSR", Report No. 2816-ARPA (Rand Corp, 1981)
92. Smith H V (Jr.), Allison P, Sherman J D *IEEE Trans. Nucl. Sci.* **32** 1797 (1985)
93. Belov A S et al. *Rev. Sci. Instrum.* **67** 1293 (1996)
94. Stockli M P et al. *AIP Conf. Proc.* **1869** 030010 (2017)
95. Hemsworth R S et al. *New. J. Phys.* 025005 (2017)
96. Belchenko Yu I et al. *Phys. Usp.* **61** 531 (2018); *Usp. Fiz. Nauk* **188** 595 (2018)
97. Belchenko Yu I et al. *AIP Conf. Proc.* **2052** 030006 (2018)
98. Dudnikov V "Modern high intensity H⁻ accelerator sources", arXiv:1806.03391
99. Dudnikov V *Istochniki Otritsatel'nykh Ionov* (Negative Ion Sources) (Novosibirsk: NSU, 2018); Dudnikov V *Development and Applications of Negative Ion Sources* (Berlin: Springer, 2019)
100. Fantz U, Lettry J *New J. Phys.* **20** 060201 (2018)
101. ITER Neutral Beam Test Facility — 2017, https://www.youtube.com/watch?v=DKOHJYxK15o